OPTIMIZING BAT CARCASS SEARCH AREAS USING A CFD-LAGRANGIAN MODELING APPROACH

by

J. Ezequiel Martin, Marcela S. Politano, Shivendra Prakash,
Pablo M. Carrica and Corey D. Markfort

Submitted to

MidAmerican Energy Company

Limited Distribution Report No. 414

FINAL REPORT

IIHR – Hydroscience & Engineering
College of Engineering
The University of Iowa
Iowa City, Iowa 52242-1585

January 5, 2017

Executive Summary

A numerical model is developed to simulate the interaction of bats with an operational utility-scale wind turbine. The model can predict instances where bats are struck by wind turbine blades and ultimately where carcasses land on the ground. The model can be used to estimate the rate at which different bat species may be impacted by wind turbines and landing locations. Model results may be used to define carcass search areas, correct survey data to account for unsearched areas around turbines and to test possible mitigation strategies. Using SCADA data with nearby meteorological data and comparing with bat carcass surveys conducted at Iowa wind farms, the most likely conditions when bats are impacted by turbines can be quantified. Using a computational fluid dynamics code (SOWFA), developed at the National Renewable Energy Laboratory, with an offline particle dynamics code, developed at IIHR-Hydroscience & Engineering, bat trajectories are modeled considering variations in wind speed, turbine operation, and bat characteristics. The model is compared to field data for the survey campaigns of 2015 and 2016 at the Lundgren and Macksburg wind farms, and is used to estimate the total mortality by correcting the field data to unsearched areas. Limitations and future improvements are discussed.

Acknowledgements

This study was conducted for MidAmerican Energy Company (MEC). The authors are grateful to Jesse Leckband, Sr. Environmental Analyst at MEC for his insight and contributions to this project.

TABLE OF CONTENTS

Page

EXECUTIVE SUMMARY I

ACKNOWLEDGEMENTS II

TABLE OF CONTENTS III

LIST OF TABLES V

LIST OF FIGURES VI

1 INTRODUCTION 1

2 GOALS AND OBJECTIVES 2

3 LITERATURE REVIEW 3

3.1 Bat Carcass Surveys 3
3.2 Characteristics of Bats Impacted by Wind Turbines in Iowa 4

4 MODELING 6

4.1 Turbine Flow Modeling 6
4.2 Bat Tracking Model 7
4.2.1 Transport Model 8
4.2.2 Model Parameters 10

5 ESTIMATION OF DRAG COEFFICIENT AND COEFFICIENT OF RESTITUTION ... 12

5.1 Drag Coefficient C_d 13
5.2 Coefficient of Restitution e 16

6 SIMULATION OF BAT TRAJECTORIES FOR A TYPICAL TURBINE OPERATION 16

6.1 Simulation Conditions 16
6.1.1 Operational Curve for Siemens Wind Turbines 17
6.2 Numerical Domain 19
6.3 CFD Grid 20
6.4 Flow Field around the Turbine 21
6.5 Bat Trajectories and Carcass Distribution 21
6.6 Other Aerodynamic Effects 28
6.6.1 Effects of Flow Variability. 29
6.6.2 Effects of Turbine Rotational Speed 32

7 COMPARISON AGAINST FIELD DATA 33

7.1 2015 Survey 34
7.2 2016 Survey 39

7.3 2015 and 2016 Survey Data Comparison 43
7.4 Comparison of Survey Data with Simulation Results 45

8 CONCLUSIONS AND FUTURE WORK..... 51

9 REFERENCES 53

LIST OF TABLES

Page

Table 3-1 Physical and Behavioral Characteristics of Bats 6

Table 5-1 Bat Physical Properties 14

Table 5-2 Drag Coefficient (C_d) range for different bat species 15

Table 5-3 Coefficient of Restitution (e) Range for Different Bat Species 16

Table 6-1 Bat Species and Parameters Analyzed 22

Table 7-1 Total Number of Turbines in each Group 40

LIST OF FIGURES

Page

Figure 4-1 Percentage of impacts as a function of strength of repulsive force..... 11

Figure 4-2 Percentage of impacts as a function of search radius size. Black lines shows solidity; surface grid size is the same for all cases. 11

Figure 4-3 Particle trajectories, stationary surfaces, for C_R = 0.14 (0.6% impacts) and 0.2 (no impacts)..... 12

Figure 5-1 Experimental setup to measure the carcass drag coefficients. 13

Figure 5-2 Cd vs Re for different shapes (From F. M. White, Fluid Mechanics, Chapter 7, 7th Edition). 15

Figure 6-1 Siemens 2.3 MW operation curve based on SCADA data..... 19

Figure 6-2 Numerical domain and boundary conditions. 19

Figure 6-3 Numerical grid. 20

Figure 6-4 Velocity distribution around the turbine predicted with SOWFA. 21

Figure 6-5 Trajectories of Indiana bats flying with relative velocity of 4.8 m/s with $C_D = 0.4, e = 0.8$ (left) and $C_D = 1.2, e = 0.2$ (right)..... 22

Figure 6-6 Bat carcass distribution for Indiana bats flying with the wind into the turbine with relative velocity of 4.8 m/s..... 23

Figure 6-7 Bat carcass distribution for Indiana bats flying with the wind into the turbine with relative velocity of 2.4 m/ (right) and spatial and cumulative distribution as a function of the distance to the tower (left)..... 24

Figure 6-8 Bat carcass distribution for Indiana bats flying with the wind into the turbine with relative velocity of 0 m/s..... 24

Figure 6-9 Bat carcass distribution for Indiana bats flying with the wind (left) and against the wind (right) for masses of 5 g (top), 8 g (center) and 11 g (bottom). 26

Figure 6-10 Bat carcass distribution for 28 g Hoary bats flying from different directions respect to the turbine at 7 m/s relative to the wind..... 27

Figure 6-11 Impacts (top) and carcass distributions for bats hitting the rotor below hub height (bottom left) and above hub height (bottom right) for 28 g Hoary bats flying at 7 m/s relative to the wind..... 28

Figure 6-12 Incoming logarithmic velocity profile 30
Figure 6-13 Histogram and cumulative as a function of the distance to the tower, for uniform incoming velocity (blue), logarithmic profile (orange) and logarithmic profile with random fluctuation superimposed to mean profile (green)..... 30
Figure 6-14 Turbulent kinetic energy (k, left) and dissipation rate (e, right) for logarithmic profile incoming velocity. Turbine rotor center is located at (x,z) = (0,0) in plots. 32
Figure 6-15 Fluctuation intensity as a function of the local velocity (left) and integral timescale (right) for logarithmic profile incoming velocity. Turbine rotor center is located at (x,z) = (0,0) in plots. 32
Figure 6-16 Histogram and cumulative as a function of the distance to the tower, for 8.25 RPM (blue), 9.64 RPM (orange) and 11.0 RPM (green). 33
Figure 7-1 Histogram (top) and cumulative (bottom) as a function of the distance to the tower for all bat species at Lundgren and Macksburg wind farms for the 2015 survey..... 35
Figure 7-2 Spatial distribution of all bat carcasses found in surveys conducted at Lundgren and Macksburg wind farms in 2015. 36
Figure 7-3 Typical Lundgren pad and access road. 37
Figure 7-4 Measured and predicted histograms for the search area (pad+road) for Lundgren (top) and Macksburg (bottom) for 2015 survey. 38
Figure 7-5 Measured and predicted histograms for the total circumferential area for Lundgren (top) and Macksburg data (bottom) for 2015 survey. 39
Figure 7-6 Histogram (top) and cumulative (bottom) as a function of the distance to the tower for all bat species at roads/pads in Lundgren and Macksburg wind farms for 2016 survey. 41
Figure 7-7 Histogram (top) and cumulative (bottom) as a function of the distance to the tower for all bat species at square plots in Lundgren and Macksburg wind farms for 2016 survey. 42
Figure 7-8 CDF comparison between Road/Pad and Square plots 43
Figure 7-9 CDF comparison between 2015 and 2016 surveys 43
Figure 7-10 Carcass distribution in 2015 (top) and 2016 (bottom) surveys 44
Figure 7-11 Lundgren and Macksburg data for 2016 campaign (pad and road turbines only). .. 46

Figure 7-12 Measured and predicted radial distributions at pads and roads for Lundgren (top) and Macksburg (bottom) for 2016 survey. 47

Figure 7-13 Histograms for the total circumferential area including corrected Lundgren data (top), Macksburg data (bottom) and model predictions for each case, for 2016 survey. 48

Figure 7-14 Combined Lundgren and Macksburg data for 2016 campaign near the turbine tower. "Pad and access road" turbine group data have been scaled by a factor of 3.05 for comparison to data from "Square plots" turbine group. 49

Figure 7-15 Combined Lundgren and Macksburg data for 2016 campaign (all distances). "Pad and access road" turbine group data have been geometrically corrected, and scaled by a factor of 3.05 for comparison to data from "Square plots" turbine group. ... 50

Figure 7-16 Combined Lundgren and Macksburg data for 2016 campaign Relative search efficiency between "Pad and access road" turbine group (geometrically corrected and scaled by a factor of 3.05 for comparison) to "Square plots" turbine group. 50

1 INTRODUCTION

Wind turbines have been found to impose a risk on wildlife, including birds and bats, as a result of collisions with turbine blades and associated infrastructure (Howell and DiDonato 1991, Hall and Richards 1972). Recent studies indicate that, in the Midwest and Eastern United States, far more bats than birds are killed by wind energy facilities (Pruitt and Okajima, 2014). In fact, bat mortality has been reported at each wind facility studied to date (GAO 2005, Kingsley and Whittam 2007, Kunz et al. 2007, Kuvlesky et al. 2007, NAS 2007, Arnett et al. 2008). There is limited data about the behavior of bats in the proximity of wind turbines. However, some studies indicate bats may be attracted to turbines, increasing the risk of bat strike by turbine blades. There is some evidence that bats may be drawn to wind turbines, either due to sound produced by the turbines (Horn et al. 2008) or insects that concentrate around the turbines (Kunz et al. 2007). Additionally, turbines extract energy from the wind leading to enhanced turbulence and reduced velocity downwind of the turbine blades (Zhang et al. 2012). This leads to a sudden drop in pressure across the turbine rotor, which has been demonstrated to result in barotrauma and possibly death to bats (Baerwald et al. 2008).

Bats generally emerge in the evening around dusk to feed on insects in the understory of forested areas. There is reduced risk of bat-turbine interactions under these conditions because wind farms generally are not located near forests and rivers corridors, which tend to provide good habitat for bats. However, during seasonal migration, and particularly in the late summer to early autumn, the risk to bats interacting with wind farms increases. It is likely that the majority of bats killed at wind farms will occur during this period (Johnson 2005, Kunz et al. 2007, Arnett et al. 2008).

It is not possible to prevent all bat deaths due to turbines and associated infrastructure, however bats placed on the Threatened and Endangered Species List must be permitted and monitored to ensure allowable mortality rates are not exceeded. Three bat species of particular concern in the Midwest region are the Indiana Bat, Northern Long-Eared Bat and Little Brown Bat; the first species is listed as Endangered and the second is listed as Threatened.

The US Fish and Wildlife Service is responsible for permitting and monitoring bat mortality at wind farms. Current strategies employed to survey a wind farm for possible bat deaths involve

searching the ground for bat carcasses within a specified radius around wind turbines. Guidance for prescribing the search radius around turbines is based on limited data, possibly leading to surveys being conducted where bats are unlikely to be found or alternatively limiting search areas and possibly missing bat carcasses that land outside the survey zone (Hull and Muir 2010, Huso and Dalthorp 2014).

There is a need for a reliable method to assess the extent and likely locations where bat carcasses may be found around turbines to help guide survey efforts. This report outlines a physics-based approach that can accurately model the interactions between bats and wind turbines, detect blade strike, and track where bat carcasses land on the ground. Results from this approach can be used to define search areas, and to correct survey data to account for unsearched areas around turbines. A technically defensible survey is a critical component to determine whether wind turbines adversely affect listed species and to evaluate project impacts.

2 GOALS AND OBJECTIVES

IIHR – Hydroscience & Engineering (IIHR) has developed a numerical modeling framework to evaluate and address the potential impact of wind turbines on bats, and determine the most likely locations where bat carcasses may be found. The primary objective of the model study described in this report is to determine the sampling area where the carcasses of bats are likely to be present after collision with a wind turbine. As a first approximation, bats are represented as particles without behavioral response. Bats are assumed to approach the front of the rotor with a uniform probability. The tasks involve in this study are summarized as follows:

1. Perform a literature review to determine constraints characterizing under what meteorological conditions bats are most commonly impacted by turbine blades, and determine the flight and fall characteristics of bats.
2. Perform CFD simulation of a turbine operating with a single wind speed and direction.
3. Estimate drag coefficient and coefficient of restitution for bat carcasses from measurements.

4. Perform particle-tracking simulations to determine the spatial distribution of bat carcass deposition, assuming an equal probability of turbine blade strike across the rotor area. Use results to develop an idealized distribution map that can be used to plan carcass surveys.

5. Perform particle tracking simulations to determine bat carcass deposition as a function of migration altitude.

3 LITERATURE REVIEW

3.1 Bat Carcass Surveys

There are significant variations in the size of prescribed carcass search areas (Sterner 2002, Kunz et al. 2007). Gauthreaux (1996) suggested that the search area should be circular, with minimum radius proportional to the height of the turbine. The recommendation utilized results from Winkelman (1989, 1992) and prescribed the search area within 70 m of turbines. AusWind (2005) suggested that the search area should have a radius equivalent to the height of the turbine. Hull and Muir (2010) review the variety of search distances used in previous research. Recently, many studies have implemented the criteria for the size of fall zone of birds and bats to quantify the carcass search area (Erickson et al. 2004, Arnett 2005, Smallwood and Thelander 2005 & Hotker et al. 2006). For estimating the search zone, Osborn (2000) performed experiments by dropping bird carcasses from wind turbine nacelle and upper limits of the swept area of wind turbine blades, on days with brisk wind. The different guidelines for search area quantification in past studies indicate that search areas are based on a heuristic understanding of where bat carcasses may be found and could be improved based on more rigorous scientific understanding. It is likely that insufficient search areas may lead to biased estimates of bat carcasses.

Huso and Dalthorp (2014) review the various sources of uncertainty for bat carcass surveys below turbines and surrounding areas within the search zone. They report that the sources of uncertainty come from carcasses falling into unsearched areas or inaccessible areas, carcasses removed or destroyed by scavengers before sampling and carcasses in the search area missed by the surveyors. Hull and Muir (2010) and Kunz et al. (2007) emphasized the need for quantification of the bat carcasses within the search zone providing a reliable estimate of bat mortalities. An

estimate of the maximum distance that bat carcasses fall away from the turbine base is essential for the comparison of the various studies at different wind farms.

The above description outlines the different approaches and criteria applied to model the search area around turbines and source of the associated uncertainties. This emphasizes the need for a model that describes the search area for bats of different physical/behavioral features colliding with different sized wind turbines. Hull and Muir (2010) hypothesized that search radius around turbines is a function of turbine height, rotor rotation rate, and size of bats. Bats approaching the turbine from different directions and with different relative velocities are likely to be struck by wind turbines with different frequency and the spatial distribution of carcasses post-collision will likely vary as well. It will be useful to optimize survey strategies based on knowledge about where bat carcasses are most likely to be found.

3.2 Characteristics of Bats Impacted by Wind Turbines in Iowa

The physical and behavioral properties of bats are important parameters for understanding how bats interact with turbines and where carcasses may ultimately be found on the ground after impact with turbine components. These physical properties include mass, dimensions, coefficient of restitution (e), and drag coefficient (C_d) of bat bodies. Behavioral characteristics include flight speed of the bats and the wind speed at which bats are most active.

The mass of bat species is important as it governs the weight, which is one of the components in force balance describing the movement of bats. Heavy bat species will be confined in the area closer around a turbine after collision whereas lighter species will fall farther away from turbines. The dimensions of bats (length and wingspan) can be used to account for the area of the flying bats, which is used with the drag coefficient for calculating the drag force. Bats have the greatest area when their wings are stretched in flaring position and least area with their wing folded back. The higher the area exposed to the turbine during strike, the higher will be the drag force on the bat. C_d determines the terminal velocity and hence governs time before the bat carcass hits the ground. The higher the drag coefficient, the more time the bat carcass will take to eventually reach the ground and consequently covers more distance post-collision.

The mechanics of the impact with turbine components is also important for determining the trajectory of the bat after collision. The primary parameter used to describe the dynamics of collision is the coefficient of restitution, which describes the way energy is transferred from the

turbine to the bat. The value of *e* is between zero and one. A value of one signifies that the object bounces off the colliding surface and loses no energy, or in other words the collision is perfectly elastic. A value of zero represents a collision that is perfectly inelastic; meaning all the energy of the bat is lost during impact. It combines multiple factors, for example, orientation of the animal in flight, the nature of blade strike on animal and animal's contact time with blade. The flight speed of bats incorporates the initial pre-collision velocity, which affects the *e* value depending upon the type of collision. Higher magnitude of pre-collision velocity will result in inelastic collision (low value of *e*) leading to less energy transfer and hence less distance travelled after strike.

There is limited data available for the aerodynamics coefficients for different bat species, and in fact only a limited number of studies provide data for any bat species. Noberg (1976) reported the drag coefficient of a long eared bat in horizontal flapping flight varies between 0.4 and 1.2. Very limited data exists for the impact characteristics of living organisms and none for vertebrate species. Taylor et al. (2010) estimated the restitution coefficient of mantis shrimp's telson as 0.56 with the uncertainty of ±0.083. Burgin et al. (2014) calculated the coefficient of restitution of human articular cartilage with mean value 0.502 and standard deviation being ±0.066. Coburn et al. (2013) suggested the restitution coefficient value of 0.47-0.69 for motile cells. Thielen et al. (2015) studied the impact behavior of freeze-dried and fresh pomelo peels and suggested the restitution coefficient range of 0.27-0.62. Based on the restitution coefficient values of living organisms/ tissues suggested in the above studies, the range 0.2-0.8 was selected for restitution coefficient in all bat species.

The values of the mass, length, wingspan, flight speed and wind speed of the bat species under consideration were obtained from various sources, including journal papers and reports are presented in Table 3-1.

Table 3-1 Physical and Behavioral Characteristics of Bats

	Mass (g)	Length (mm)	Wingspan (mm)	Flight speed (m/s)	Wind speed (m/s)	Drag coefficient (Flying)	Coefficient of Restitution
NLEB	6-9 [10]	76-88 [1]	230-260 [10]	2.35 [60]	<6.9 [40]	0.4-1.2 [39]	0.2-0.8 [9], [16], [53], [55]
Little Brown	5-14 [18]	60-102 [18]	222-269 [18]	11.2 [27]	4-4.5 [24]	0.4-1.2 [39]	0.2-0.8 [9], [16], [53], [55]
Indiana	5-11 [56]	70.8-90.6 [56]	240-267 [56]	4.8 [50]	5-6.9 [8]	0.4-1.2 [39]	0.2-0.8 [9], [16], [53], [55]
Hoary	20-35 [48]	130-150 [48]	342-435 [48]	<=7 [22], [47]	<4.6 [22], [15]	0.4-1.2 [39]	0.2-0.8 [9], [16], [53], [55]
Eastern Red	7-13 [1], [6]	93-117 [1], [6]	290-332 [1], [6]	6.7 [47]	8.9-10.1 [26]	0.4-1.2 [39]	0.2-0.8 [9], [16], [53], [55]
Big Brown	11-23 [21], [6]	110-130 [6]	325-350 [6]	9.5 [62]	3-7 [45]	0.4-1.2 [39]	0.2-0.8 [9], [16], [53], [55]
Silver-Haired	8-12 [6]	90-115 [6]	270-310 [6]	4.8-5 [63]	NA	0.4-1.2 [39]	0.2-0.8 [9], [16], [53], [55]
Evening Red	6-14 [7], [35]	85-105 [7], [35]	260-280 [7], [35]	4.5 [62]	NA	0.4-1.2 [39]	0.2-0.8 [9], [16], [53], [55]
Tri-Colored	4.6-7.9 [19]	77-89 [19]	220-250 [19]	NA	NA	0.4-1.2 [39]	0.2-0.8 [9], [16], [53], [55]

NA: Not Available

4 MODELING

4.1 Turbine Flow Modeling

The open source code "Simulator fOr Wind Farm Application" (SOWFA) (Churchfield et al. 2012a), developed by the National Renewable Energy Laboratory (NREL), was used to simulate the unsteady flow and turbulence around a wind turbine. SOWFA is based on the three-

dimensional Computational Fluid Dynamics (CFD) code OpenFOAM (Churchfield et al. 2012b). Turbulence closure in OpenFOAM is possible using Reynolds-Averaged Stress (RAS) or Large Eddy Simulation (LES) models. In RAS, the Reynolds Stress is modeled using standard two equation turbulence models or a Reynolds Stress equation model.

SOWFA includes an actuator line turbine model (ALM) in the library pisoFOAM to predict the wake, tip, root and blade-bound vortices. Blades are simplified as a series of lines of constant airfoil, chord, and twist angle (Sørensen and Shen 2002) and body forces from the rotor are distributed on these lines. Forces are computed from the chord length of the blade, relative blade-air velocity and drag and lift coefficients, which are provided as tabulated airfoil data. Previous studies have demonstrated the ability to accurately reproduce the turbulent flow characteristics around wind turbines using the ALM approach to represent the effect of wind turbines on the flow field (Sørensen and Shen 2002, Lu and Porté-Agel 2011). The advantage of this method is that a very fine grid around turbine blades is not required, considerably reducing computational time. However, the ALM method cannot reproduce details about boundary layer turbulence or pressure gradients around the blades as these effects are parameterized as aerodynamics forces. In addition, lift and drag airfoil data, obtained from experiments or single numerical tests, can be an important source of numerical inaccuracy.

OpenFOAM solves the continuity and momentum equations:

$$\nabla \cdot (\boldsymbol{U}) = 0 \tag{1}$$

$$\frac{\partial(\boldsymbol{U})}{\partial t} + \nabla \cdot (\boldsymbol{U}\boldsymbol{U}) = -\frac{1}{\rho}\nabla p + \nabla \cdot \boldsymbol{\tau} - 2\boldsymbol{\Omega} \times \boldsymbol{U} + \frac{1}{\rho}\boldsymbol{f}_T \tag{2}$$

where $\boldsymbol{U}$ is the velocity, p is the pressure, ρ the density and $\boldsymbol{\tau}$ the shear stress. The terms on the left hand side (LHS) of the equal sign represent accelerations, and the first two terms on the RHS represent forces due to pressure field and viscosity. The last two terms on the RHS represent the Coriolis and aerodynamic forces from the blades.

4.2 Bat Tracking Model

A particle tracking code was developed to track the motion of bats in the CFD velocity field, to estimate bat impact statistics and carcass fate after impact. A brief description of the model and implementation for bat tracking is presented here, along with some preliminary results that illustrate the capacities of the solver.

4.2.1 Transport Model

Bats are modelled as Lagrangian entities subject to interaction with fluid forces and with the turbine blades through impact and flow-induced pressure. The particle tracking technique, which takes into account the characteristics of bats, such as their mass, lift, thrust, pressure force, and drag is used to compute their trajectory. A similar technique was extensively used to simulate fish trajectories for hydropower studies (Politano et al. 2012, Goodwin et al. 2014, Romero-Gomez and Richmond, 2014). A statistically significant number of bat strike events needs to be simulated to determine bat carcass distribution patterns.

The tracking code incorporates three different elements into the calculation. The CFD solution generated with SOWFA is read and for each particle, at each time step of the particle simulation, the fluid velocity at the particle position is interpolated both in time and space. Based on the provided rotation rates for the different surfaces in the domain (blades, hub, and nacelle), the position of each surface is also updated at each particle time step. Finally, the particles' trajectory is integrated based on the external forces acting on it (drag, gravity) and those generated by the bat as it flies before the impact (thrust, estimated as equal in magnitude to the force needed to balance drag for a preset terminal velocity of advance for the bat), and lift to counteract the bat's weight. After impact, these two "internal" forces disappear.

The bats are considered as particles that respond to the fluid and have their own thrust and lift forces to fly. The force balance on a bat is:

$$\rho_P V_p \frac{d\boldsymbol{u}_p}{dt} = -V_p \nabla p + \boldsymbol{F}_D + \left(\rho_P - \rho_o\right) V_p \boldsymbol{g} + \boldsymbol{F}_R + \boldsymbol{F}_T + \boldsymbol{F}_L \qquad (3)$$

where the LHS term is the bat acceleration, the first term on the RHS is the force induced by fluid pressure gradients, and the third term on the RHS is the gravitational pull. $\boldsymbol{F}_T$ and $\boldsymbol{F}_L$ represent the bat thrust and lift forces, respectively. $\boldsymbol{F}_R$ is a repulsive force to prevent the bats from hitting static or slowly moving surfaces, as this behavior is natural and well-studied. The drag force $\boldsymbol{F}_D$ can be obtained from:

$$\boldsymbol{F}_D = -\frac{3}{4}\frac{\rho_o C_D}{d_p}\left(\boldsymbol{u}_p - \boldsymbol{u}\right)\left|\boldsymbol{u}_p - \boldsymbol{u}\right| \qquad (4)$$

where d_p is a characteristic size (a typical bat diameter). The drag coefficient C_D depends on the flow regime and particle shape. In this study, characteristic bat size and drag coefficient are used. Accounting for the particular bat shape during flight and after collision with a blade is proposed as future model improvement.

The trajectory after impact with a blade is computed as an inelastic collision. In the inertial earth system the bat velocity before the collision is $\boldsymbol{u}_p$, and the blade moves with a velocity $\mathbf{u}_B = \boldsymbol{\omega} \times \mathbf{r}$, where $\boldsymbol{\omega}$ is the rotational speed of the turbine rotor, and $\mathbf{r}$ is the vector joining the rotor shaft with the impact point along the blade. Before the collision, the bat velocity in the blade system of reference is:

$$\mathbf{v}_b = \boldsymbol{u}_p - \boldsymbol{u}_B \tag{5}$$

The collision point has an outward unit normal $\mathbf{n}$. The normal and tangential components of the bat velocity before the impact are $\mathbf{v}_{bn} = (\mathbf{v}_b \cdot \mathbf{n})\mathbf{n}$ and $\mathbf{v}_{bt} = \mathbf{v}_b - \mathbf{v}_{bn}$, respectively. The bat velocity after impact in the blade system of reference is:

$$\mathbf{v}_a = -e\mathbf{v}_{bn} + \mathbf{v}_{bt} \tag{6}$$

where e is the coefficient of restitution. In the earth reference frame the velocity is then:

$$\mathbf{u}_{pa} = \mathbf{v}_a + \mathbf{u}_B \tag{7}$$

Upon impact, the particle trajectory is re-initialized, using the initial velocity after impact in Eq. (7) and a new trajectory is tracked using only external forces; the particle motion is tracked until it reaches the ground, where its position is recorded. An impact is considered to have occurred when a particle is within a pre-determined distance from a grid point defining a solid surface. This distance cannot be smaller than the distance between grid points, or otherwise particles can “pierce” through the surface. A more accurate estimation of the impact can thus be achieved by refining the surface grid as well as the impact distance parameter; however for the purposes of obtaining a distribution of carcasses around the turbine, further refining of the grids is not recommended given the associated increase in computational cost.

In Eq. (3) an optional repulsive force field is used to try to deflect particles from static or slowly moving surfaces. The force is implemented as inversely proportional to the distance

between the particle position $\mathbf{x}_p$ and the position of control points $\mathbf{x}_{CP,i}$, and only active when the particles are at a distance from a surface smaller than a predetermined search radius:

$$\boldsymbol{F}_R = -C_R \sum_i \frac{\mathbf{x}_{CP,i} - \mathbf{x}_p}{\left\| \mathbf{x}_{CP,i} - \mathbf{x}_p \right\|^2} \tag{8}$$

where C_R is a repulsion coefficient.

4.2.2 Model Parameters

To calibrate the repulsive "behavioral" force in Eq. (8), cases for a stationary turbine were simulated. The solidity for this turbine is approximately 3.1%. Using a search radius of 1% of the turbine diameter, there are 4.1 % impacts (using 1000 randomly distributed particles upstream of the turbine) when no repulsive force is used, and as the strength of such force is increased, eventually this value is reduced to zero (see Figure 4-1). Changing the search radius decreases the initial number of impacting particles as the "effective" surface of the blades decreases, but eventually the decrease occurs due to piercing of the surface, as it becomes under-resolved by the grids defining it (see Figure 4-2). Further tests changing both grid density and search radius might be necessary to improve the base state. Figure 4-3 shows trajectories of some (approximately 40 out of 1000 simulated) particles for $C_R = 0.14$ (0.6% impacts) and 0.2 (no impacts).

A few other parameters presented in Eqs. 1 through 6 are required for modeling the bats as particles. Based on available literature values, different drag coefficient were used, ranging from $C_D =$ 0.4 to 1.2 for dead bats. Previous to impact the average reported value of 0.8 was used for live bats. The restitution coefficient varies in the range $e =$ 0 to 1, but only 0.2, 0.5 and 0.8 were used in the preliminary simulations. Finally a density of $\rho_p = 1000$ kg/m3 (equivalent to fresh water) was used to relate mass to diameter, assuming spherical particles.

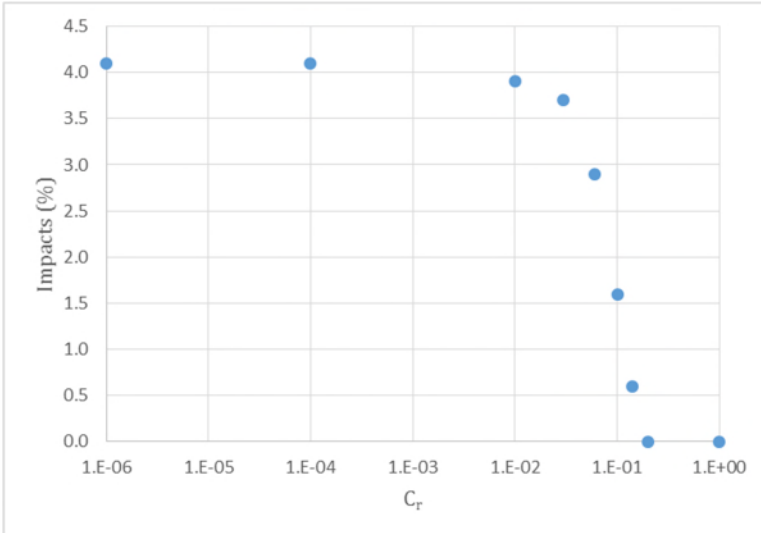

Figure 4-1 Percentage of impacts as a function of strength of repulsive force.

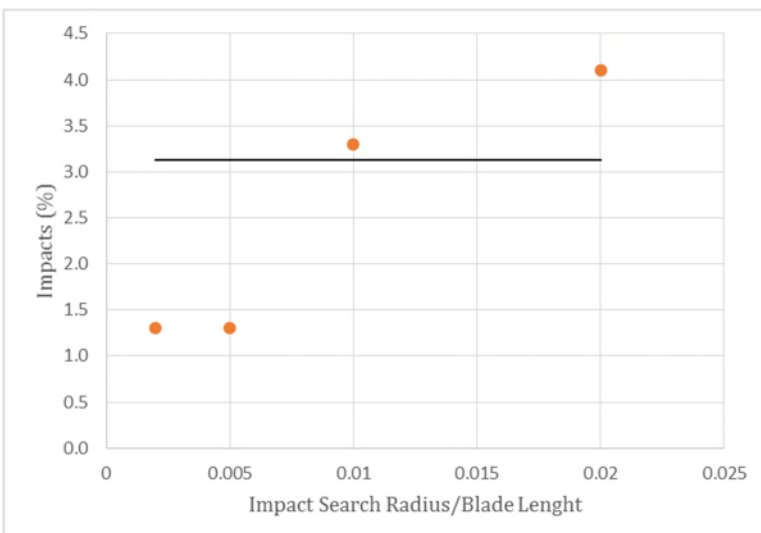

Figure 4-2 Percentage of impacts as a function of search radius size. Black lines shows solidity; surface grid size is the same for all cases.

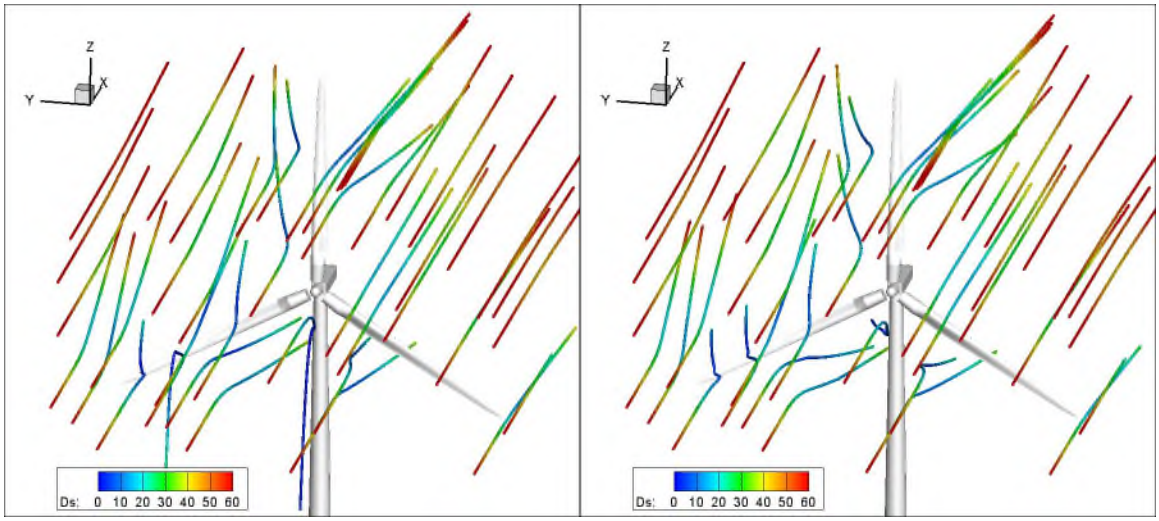

Figure 4-3 Particle trajectories, stationary surfaces, for C_R = 0.14 (0.6% impacts) and 0.2 (no impacts).

5 ESTIMATION OF DRAG COEFFICIENT AND COEFFICIENT OF RESTITUTION

As discussed in Section 3.2, the drag coefficient (C_d) and coefficient of restitution (e) are important factors required for modeling the distances that bat carcasses will travel after getting hit by wind turbine blades. The physical characteristics of bats mentioned in Table 3.1 are based on the limited published information available, in all cases for flying bats. In order to perform initial simulations, a range of C_d and e values (Table 3.1) were used for all flying bats species. C_d and e are dependent upon the mass, dimensions, and structural characteristics of the bat. For modeling the post-collision distances traversed by bat carcasses, a reliable estimate of C_d and e for individual species that takes into account size, shape and mass of the carcasses are needed.

Experiments were performed on July 21, 2016 at Macksburg wind farm, near Macksburg, IA, to estimate C_d and e for freshly discovered bat carcasses. Bat carcasses were searched on the day of the experiment and three bats of different species were found, an Eastern Red Bat, a Hoary Bat, and an Evening Bat.

5.1 Drag Coefficient C_d

The bat carcass mass and body dimensions were measured (Table 3.2). To determine C_d, the carcasses were dropped from a height of approximately 8 m. A high-speed camera was employed for recording the experiments. The carcass fell in front of a wall with distance markings taped over a distance of 4.5 m, which was used to calibrate the distance occupied in a single pixel of the captured video images, which was 7.1 mm (Figure 5-1).

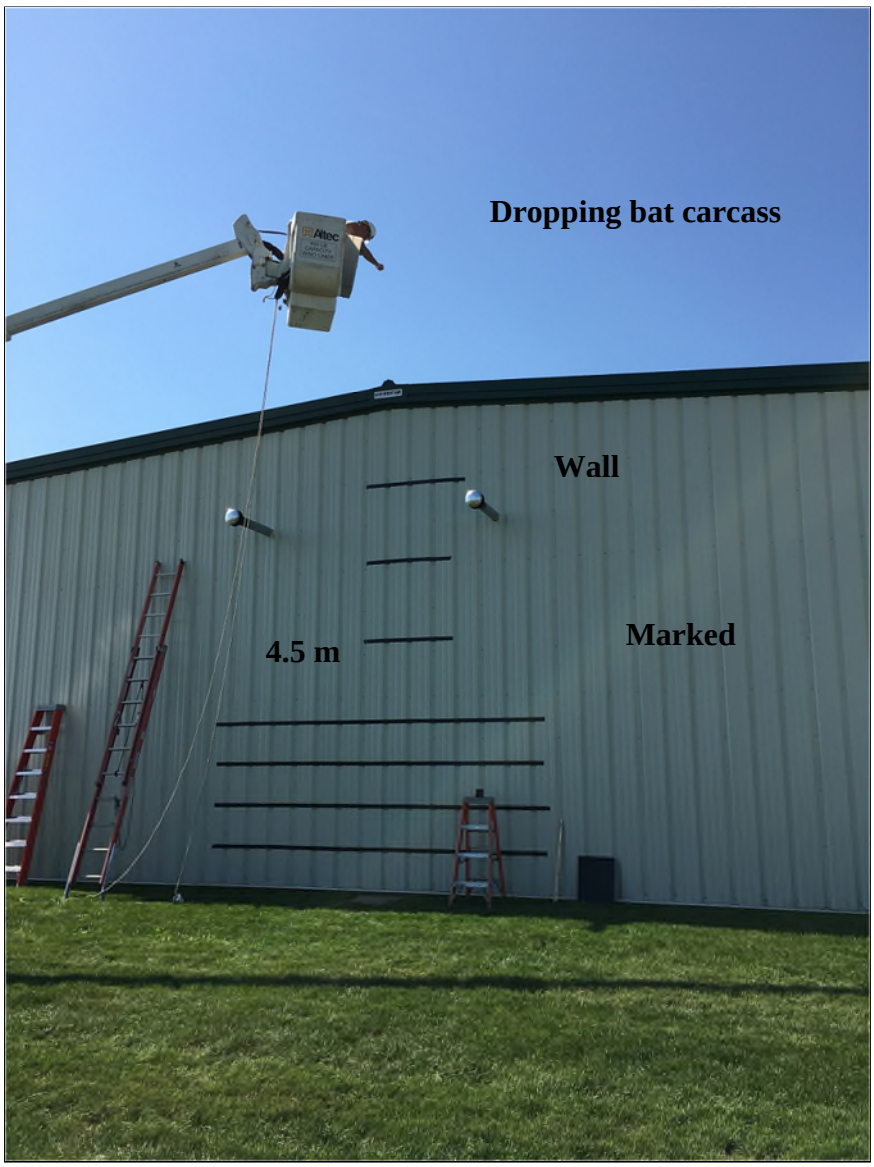

Figure 5-1 Experimental setup to measure the carcass drag coefficients.

The frames with the images obtained from the recordings were used to determine the displacement (y) over time (t) for each experiment. The temporal resolution was 0.004 sec. The bat velocity $\boldsymbol{u}_p$ at a given time was calculated using backward differences of the position measurements. For each species at least two experiments were performed and recorded. From a plot of velocity against time, it was found that the terminal velocity was not achieved for any of the experiments.

Eq. (3) applied to a carcass in a quiescent fluid results:

$$m\frac{d\boldsymbol{u}_p}{dt} = m\,\boldsymbol{g} - \frac{1}{2}\rho_o\, C_D A \boldsymbol{u}_p^2 \tag{9}$$

where m is the mass and A is the projected frontal area of the carcass. Eq. (9) can be discretized using the first-order Euler's method, resulting

$$\boldsymbol{u}_p^t = \boldsymbol{u}_p^{t-1} + \boldsymbol{g}\,\Delta t - \frac{\Delta t}{2m}\rho_o\, C_D A\left(\boldsymbol{u}_p^{t-1}\right)^2 \tag{10}$$

C_d and the initial velocity $\boldsymbol{u}_p^0$ are adjusted to obtain the best fit of Eq. (10) to the experimental data. Bat orientation, and corresponding projected area, are changing during the fall. For this study, the projected area is assumed to have an elliptical shape. The Reynolds number ($Re = \boldsymbol{u}d/\nu$, with d the bat diameter and ν the air viscosity), from which C_d depends, is calculated for a range of velocities measured during the experiments and for the range of carcass dimensions. The results are summarized in Table 5.1.

Table 5-1 Bat Physical Properties

Species Name	Mass (g)	Lengths (cm)	Projected Area (m^2)	*Re* (larger length)	*Re* (smaller length)
Evening Bat	1.5	1.905, 3.81	5.70×10^{-4}	1×10^4-2×10^4	5×10^3-1×10^4
Eastern Red Bat	9.7	2.54, 5.08	1.01×10^{-3}	2.5×10^4-4×10^4	1.2×10^4-2×10^4
Hoary Bat	24.1	3.81, 7.62	2.28×10^{-3}	3.5×10^4-5.5×10^4	1.7×10^4-2.7×10^4

The estimated range for C_d is based on fitting Eq. (10) for two drop experiments for each bat species, assuming constant C_d, and varying the fitted model from -10% to +10% of the minimum error of the best fit curve. The associated range for C_d between the two experiments is reported in Table 5.2.

Table 5-2 Drag Coefficient (C_d) range for different bat species

Species Name	C_d
Evening Bat	0.76 – 0.96
Eastern Red Bat	0.33 - 0.60
Hoary Bat	0.43 – 0.69

The method used to calculate C_d assumes that the drag coefficient is constant in the range of measured speeds. However, C_d is a function of *Re* (see Figure 5-2 for typical values for some three-dimensional bodies). For the range of experimental conditions and sizes of bat carcasses in this study, *Re* lies between 5×10^3 and 6×10^4, thus the assumption of constant C_d is valid.

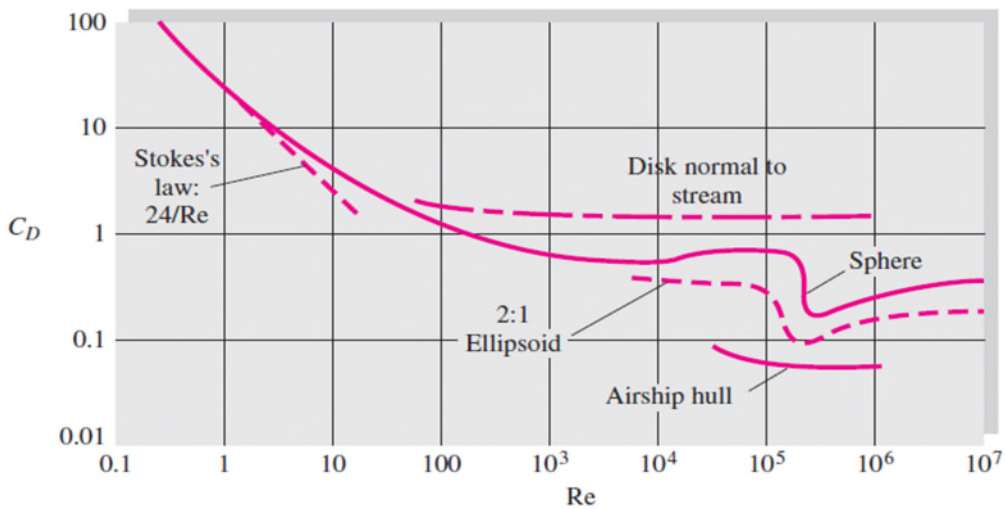

Figure 5-2 Cd vs Re for different shapes (From F. M. White, Fluid Mechanics, Chapter 7, 7th Edition).

5.2 Coefficient of Restitution *e*

The coefficient of restitution (*e*) is defined as the ratio of relative velocity after to relative velocity before collision of one object with another. It is an important parameter used in the modeling to determine how a bat carcass will "bounce" off a turbine blade after collision. To calculate *e*, bat carcasses were accelerated toward a thick rectangular metal plate, and video recorded using the high-speed camera, similar to the free-fall experiments. From the images, velocities just before and after the collision were estimated. The following table summarizes the coefficients of restitution for each bat species.

Table 5-3 Coefficient of Restitution (*e*) Range for Different Bat Species

Species Name	Coefficient of Restitution	Approximate impact velocity (m/s)
Evening Bat	0.11	15
Eastern Red Bat	0.023	17
Hoary Bat	0.1	17

It should be noted that for the Eastern Red Bat the carcass was partially decayed, which possibly led to an unrealistic small estimate of the coefficient of restitution *e*. The approximate impact velocity for the experiments to estimate *e* was between 15 – 17 m/s, which are on the same order as bats that hit the inner radius of the rotor, but may not be representative of impacts on the outer part of the rotor.

For Hoary and Evening Bats, the estimated coefficient of restitution is roughly the same, approximately 0.1.

6 SIMULATION OF BAT TRAJECTORIES FOR A TYPICAL TURBINE OPERATION

6.1 Simulation Conditions

The wind speed for highest bat activity increases the likelihood of bats colliding with turbines. Bats are generally most active in the evening when wind speeds are relatively low, often below 7 m/s. Turbines operate between a cut-in wind speed and maximum cut-out speed. Based on

observations and following MEC suggestion, the simulations were run for a wind speed of 5 m/s, which provides a high likelihood that bats will be active while turbines are operational.

An analysis was performed for a Siemens 2.3 MW turbine operating at a wind speed of 5 m/s in speed control mode. Since geometric data for the Siemens turbine is proprietary and unavailable, an NREL 5 MW turbine was scaled to match the main characteristics of the Siemens turbine. Notice that this is an approximation, even though turbine radius, RPM and power are matched, because the turbine blades are not geometrically similar, and the operational pitch will likely be different as well.

The turbine consists of 3 blades with 54 m tip radius and hub radius 1.5 m. Blades were discretized with 64 spanwise points. Overhang is 5.01910 m and tower height is 80 m.

6.1.1 Operational Curve for Siemens Wind Turbines

The operational curve of a wind turbine is a plot that indicates the output power at different wind speeds. Using SCADA data from MEC wind turbines, the RPM for the most probable wind speed at which bats are detected more frequently was determined. The wind speed and RPM data from the Lundgren wind farm was used for developing the operational curve of the wind turbines. Lundgren wind farm has 107 Siemens SWT-2.3-108 turbines, each with a nameplate capacity of 2.346 MW. The rotor diameter of the turbines is 108 m and turbine hub height is 80 m.

The wind speed and RPM data were provided in the form of an irregular time series. Linear interpolation at the interval of 10 seconds was used to convert the irregular series into the regularly spaced time series. Autocorrelation analysis of the time series yielded the integral time scale of approximately 2 minutes for RPM and 40 seconds for the wind speed. The cross correlation analysis of the interpolated RPM and wind speed time series revealed the highest correlation between the two series at a time lag of 20 seconds, which indicates that the turbine controller updates the rotation speed of the turbine at approximately 20 second interval on average.

The data was then post processed to remove large gaps in the raw time series. Based on cross correlation analysis, a 20 second moving average time series for wind speed and RPM was calculated. The interpolated RPM data was then removed for gaps greater than 20 seconds over the time frame for which gaps exist in the raw data. Similarly, the time filtered wind speed data was removed for missing data in the raw series with gaps greater than 10 seconds. After, post processing the data, RPM values less than 5 were removed as these were mostly erroneous and

likely the turbine does not operate in this range. Finally 10 seconds interpolated data followed by 20 second moving average for wind speed and RPM with further removing large data gaps and data with RPM <5, is used for deriving the operational curve (Figure 6-1).

Geographical coordinates of the turbines are used for detecting the turbines located at the edge of the wind farm as these turbines have the best quality data because they are rarely in the wake of other turbines. In Lundgren wind farm, turbines T006, T007, T008, T129 and T130 were identified as turbines that experience winds not frequently affected by upwind turbines. The operational curve equation for each of these turbines obtained using the methodology outlined above, was very similar. Therefore, the data from these turbines were combined for plotting the operational curve.

The relationship between RPM and wind speed, for RPM values between 5 and 14, can be represented by a linear model. To fit the linear model, the mean and standard deviation of the wind speeds at each of the individual RPM (5-14) was calculated. Then, using least square regression, a linear model is fitted between mean wind speed values and corresponding RPM (Figure 6-1). The best fit line is described by the following equation:

$$RPM = 0.2 + 1.7(WS) \tag{11}$$

where WS represents the wind speed. Cryan et al. (2014) suggested that bats are observed more frequently at lower wind speeds and most fatalities occur during late summer and autumn at average wind speed of 5-6 m/s. Arnett et al. (2008) also mentioned that bat fatalities are highest on nights with low wind speeds less than 6 m/s. Based on these findings, simulations were run at wind speed of 5 m/s. From, the best-fit line describing the turbine operation, the RPM value for 5 m/s wind speed is 8.7.

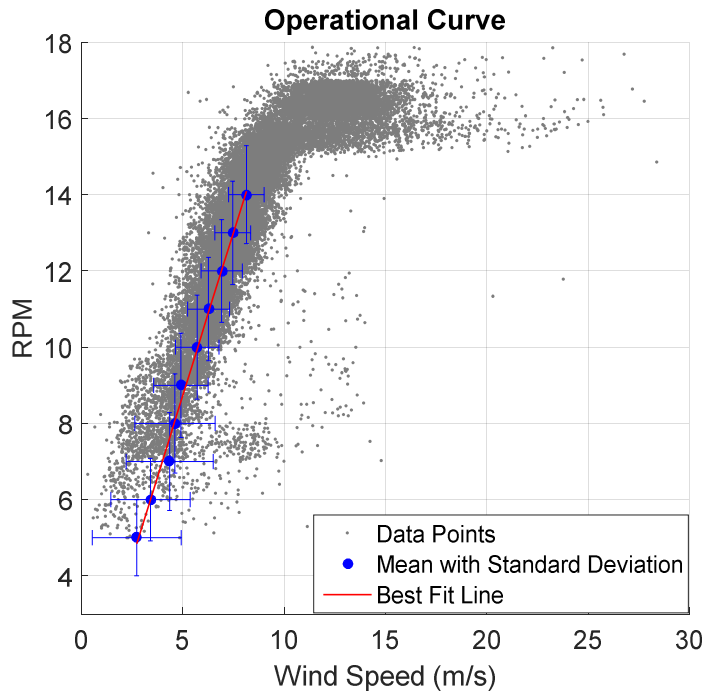

Figure 6-1 Siemens 2.3 MW operation curve based on SCADA data.

6.2 Numerical Domain

Figure 6-2 shows a schematic of the numerical domain and boundary conditions. The domain is 26 R long (with R the tip radius) and 3 R in height from the rotor hub. The turbine is located 6 R downstream from the inlet. The tower was not included or modeled in the CFD component of this study.

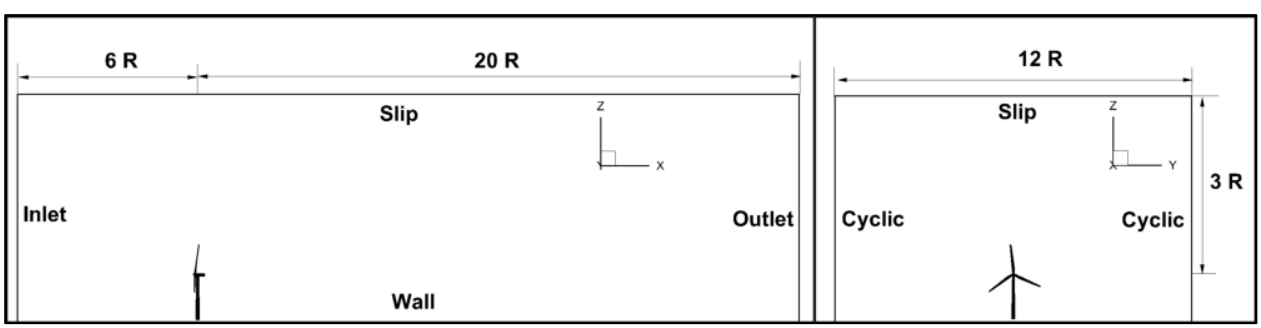

Figure 6-2 Numerical domain and boundary conditions.

The boundary conditions used were:

Inlet (west boundary condition in SOWFA): Dirichlet boundary condition (constant value) for velocity, k and epsilon. Zero gradient for pressure.

Outlet (east boundary condition in SOWFA): inlet-outlet condition (zero gradient if outlet, zero quantity if inlet) for velocity, k and epsilon. Zero gradient for pressure.

Bottom: wall non-slip condition for velocity, and wall law for k and epsilon k. Zero gradient for pressure.

Top: slip condition (zero shear stress) for velocity. Zero gradient for pressure.

6.3 CFD Grid

The grid, consisting on hexahedral blocks, was generated using the blockMesh utility of OpenFOAM. The x-direction is aligned with the flow and z-direction upwards as required by SOWFA. A Cartesian block was first generated using (195x90x90) nodes in the (x,y,z) directions. The grid was then refined 4R around the turbine, dividing grid elements in half in each direction using the OpenFOAM utility refineMesh. The final grid, shown in Figure 6-3 , contains 5.4 10^6 cells.

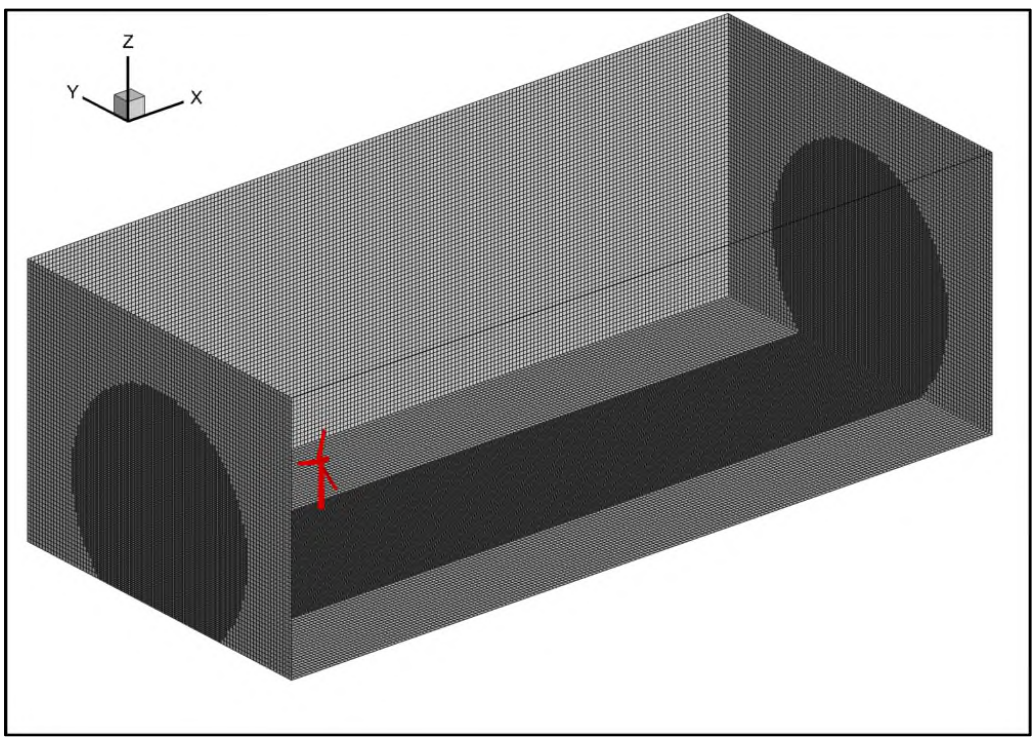

Figure 6-3 Numerical grid.

6.4 Flow Field around the Turbine

The model was run for 250 s (37 rotor revolutions) and the last 2.2 s (1/3 rotation) were saved and used to perform the particle simulations. Figure 6-4 shows the velocity magnitude deficit in the wake predicted with SOWFA at 250 s. The wake shape predicted with the model is consistent with similar simulations using SOWFA found in the literature (Oggiano 2014). High velocity deficit are predicted behind the rotor. Further downstream in the wake the region of low velocities diminishes as the wake expands. The maximum and average velocity deficit at 1 R downstream of the turbine were 0.57 and 0.37, respectively.

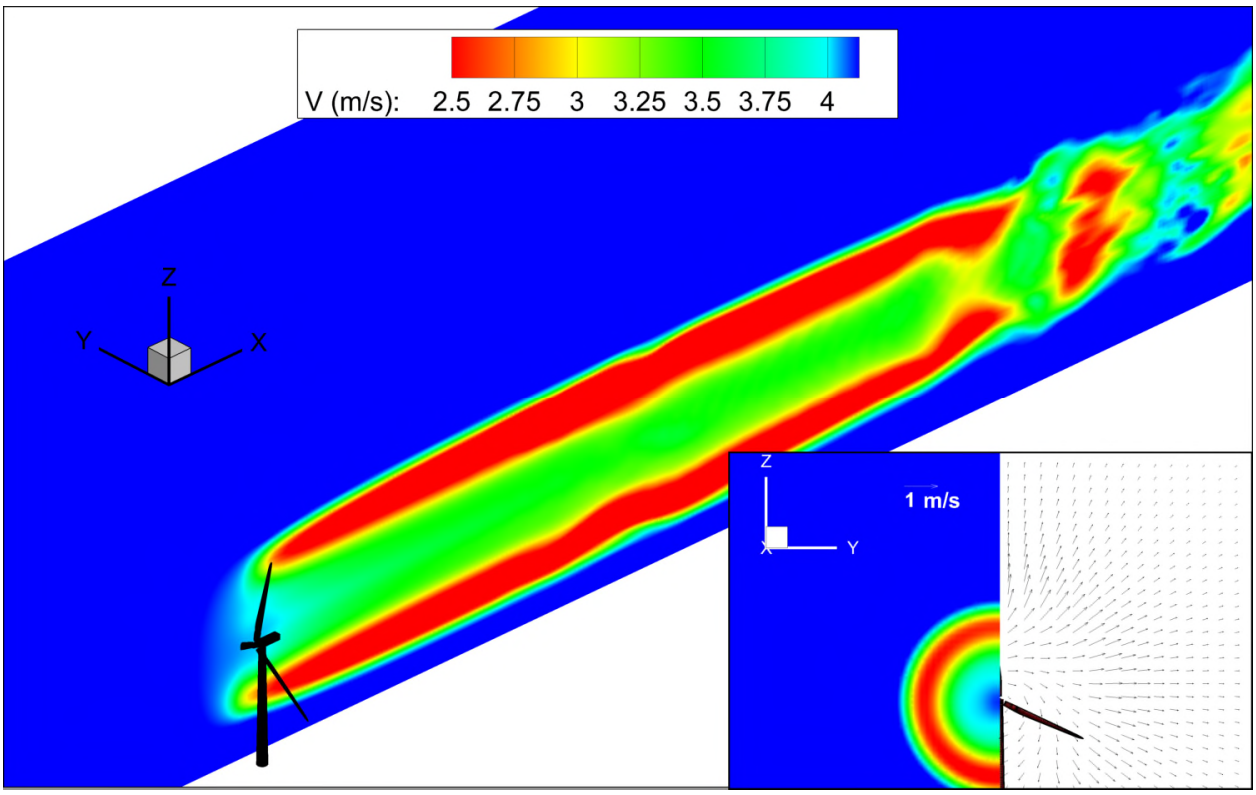

Figure 6-4 Velocity distribution around the turbine predicted with SOWFA.

6.5 Bat Trajectories and Carcass Distribution

As a preliminary evaluation of the sensitivity of the model described in §4.2 to the simulation parameters, particles with typical properties of Indiana and Hoary bats were studied. These species were selected because they are on the boundaries of the size spectrum of bats of interest, with the Indiana bat very small (approximately 8 g in weight) and the Hoary bat large (around 28 g in

weight). Table 6-1 shows parameters used in the example computations. The flow solutions presented in §6.4 were used.

Live bats are injected flying towards the turbine in any direction, and interact with the rotating blades when they reach the rotor plane. Though possibly very important, at this time effects of turbulence and bat behavior on trajectories are neglected. Turbulence modeling will be added in future simulations, while accepted bat behavior models can also be implemented if available.

Table 6-1 Bat Species and Parameters Analyzed

Species	Weight (g)	Speed (m/s, relative to wind)	Drag Coefficient live/dead (C_D)	Restitution Coefficient	Repulsion Coefficient (C_R)
Indiana bat	5, 8, 11	0,2.4,4.8	0.8/0.4-1.2	0.2, 0.5, 0.8	0.2
Hoary bat	28	7.0	0.8/0.8	0.5	0.2

Figure 6-5 shows some example trajectories of Indiana bats that are hit by the blades as they travel with the wind head on into the turbine at a relative velocity of 4.8 m/s. Results confirm the expected outcome of less bouncing off the blades with smaller restitution coefficient, and more straight-down trajectories with higher drag coefficient.

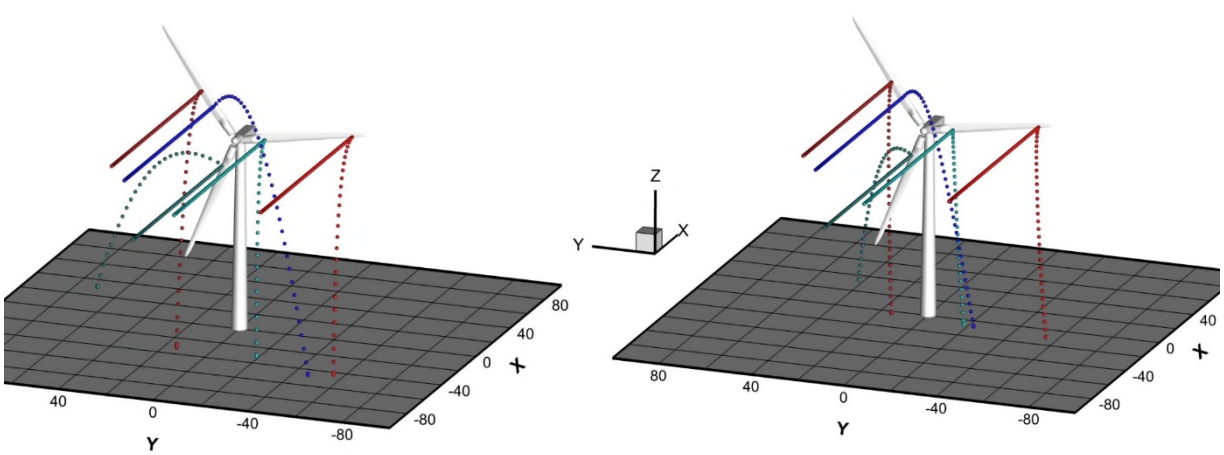

Figure 6-5 Trajectories of Indiana bats flying with relative velocity of 4.8 m/s with $C_D = 0.4, e = 0.8$ (left) and $C_D = 1.2, e = 0.2$ (right).

The effects of the flying speed on carcass distribution for 8 g Indiana bats are shown in Figure 6-6, Figure 6-7 and Figure 6-8. Results are displayed in normalized distributions in space, with the wind direction from left to right. Bats are counted in squares 16.6 m in side. As the bat velocity decreases, the exposure time to the turbine blades increases and the impact probability increases from 12.8% at 4.8 m/s relative velocity to the wind (9.8 m/s relative velocity to the turbine), to 22.5% at 0 m/s (5 m/s relative to the turbine).

An increase in restitution coefficient results in bats falling further away from the turbine, while an increase in drag coefficient results in bat carcasses concentrating closer to the tower. In the worst condition, bats can be found as far as 200 m away from the turbine, but in all cases over 90% of the bats are found within 100 m from the tower.

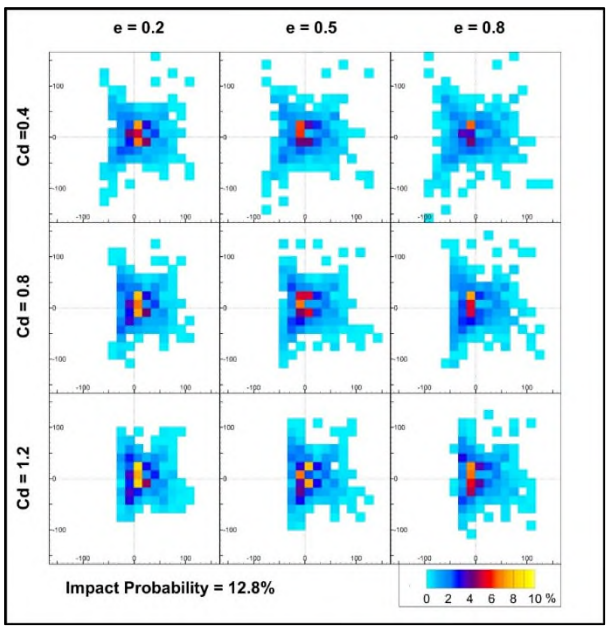

Figure 6-6 Bat carcass distribution for Indiana bats flying with the wind into the turbine with relative velocity of 4.8 m/s.

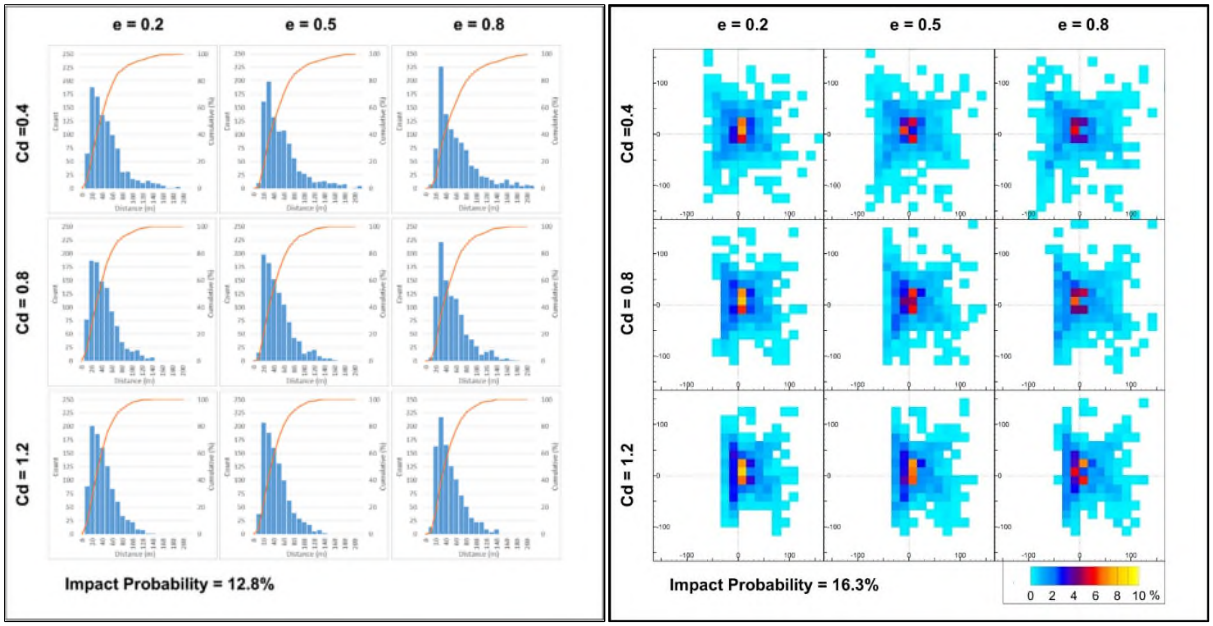

Figure 6-7 Bat carcass distribution for Indiana bats flying with the wind into the turbine with relative velocity of 2.4 m/ (right) and spatial and cumulative distribution as a function of the distance to the tower (left).

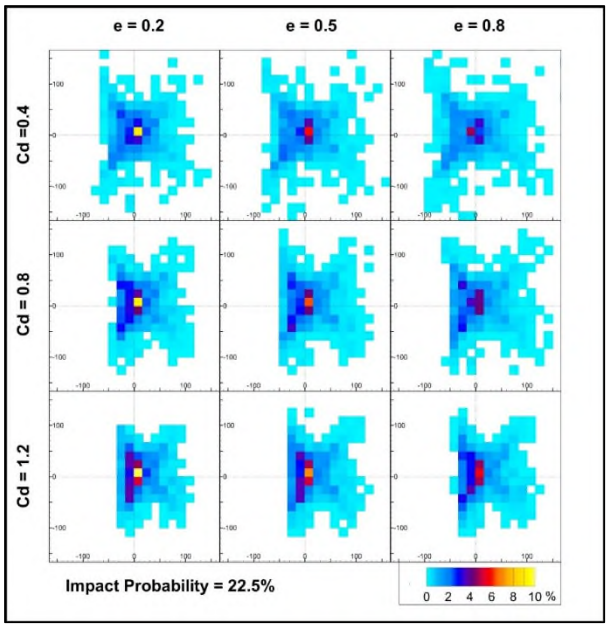

Figure 6-8 Bat carcass distribution for Indiana bats flying with the wind into the turbine with relative velocity of 0 m/s.

The effect of bat mass and migration direction with respect to wind direction is shown in Figure 6-9, where the wind direction is left to right. Because the relative velocity of the bats is 4.8 m/s, when flying against the wind bats can only approach the turbine if they are inside the wake, where the velocity is lower. The low relative velocity with the turbine results in a very high impact rate of approximately 33%, and the bats spread on a much wider pattern than when flying with the wind. It is interesting to note that heavier bats exhibit narrower distributions when flying with the wind, and wider when flying against the wind.

The Hoary bats are modeled with a mass of 28 g and a relative velocity of 7 m/s. Carcass distribution is shown in Figure 6-10 , which shows that the distributions skew in the direction of flight of the bats by about 30 m. It is also clear that very few of these heavier bats fall beyond 100 m from the tower.

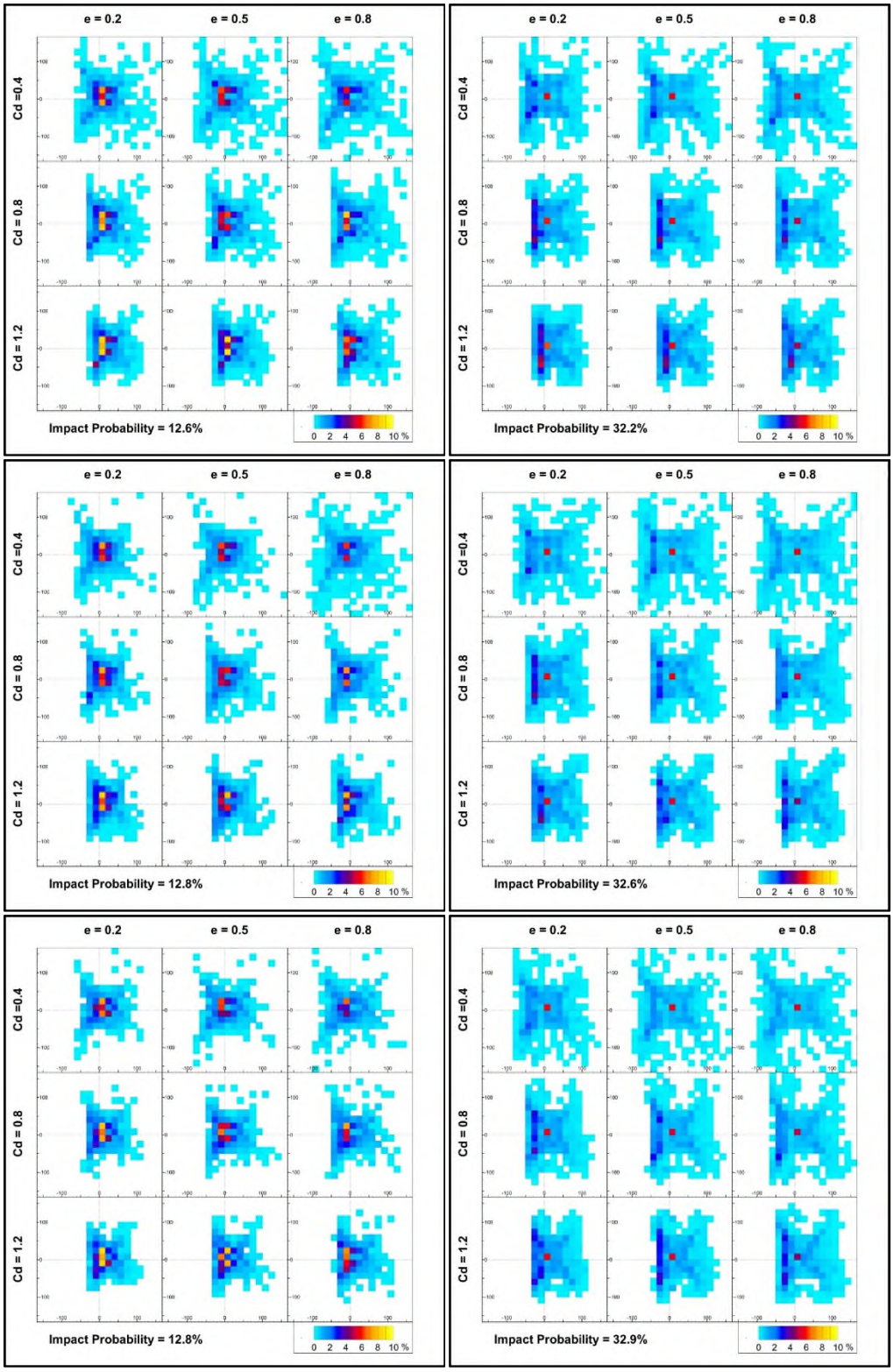

Figure 6-9 Bat carcass distribution for Indiana bats flying with the wind (left) and against the wind (right) for masses of 5 g (top), 8 g (center) and 11 g (bottom).

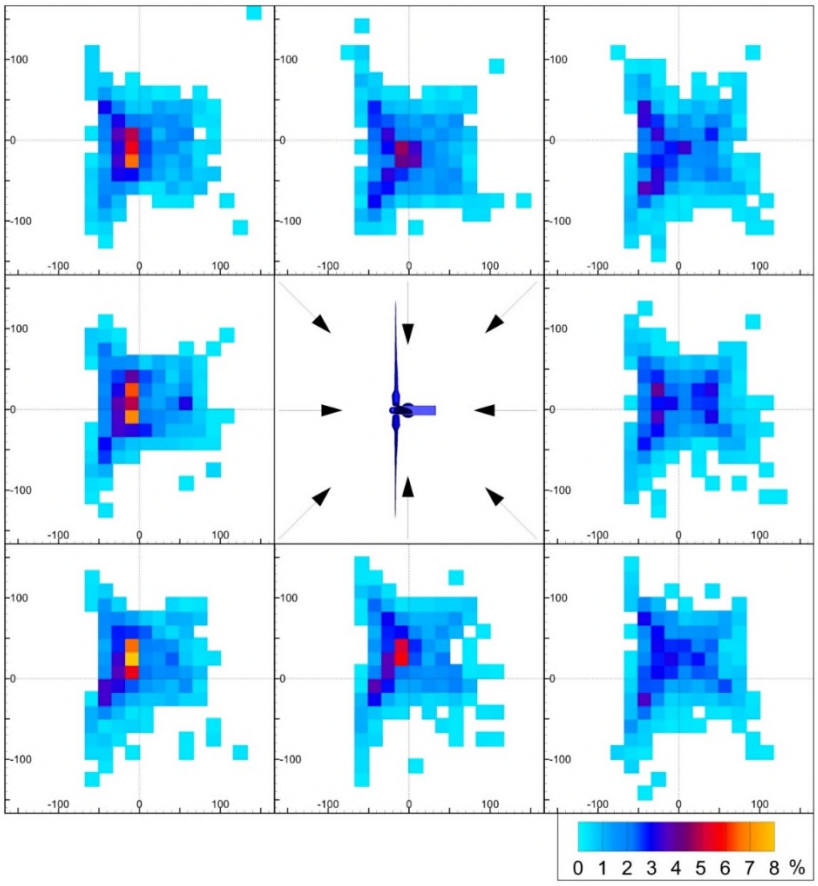

Figure 6-10 Bat carcass distribution for 28 g Hoary bats flying from different directions respect to the turbine at 7 m/s relative to the wind.

Figure 6-11 shows the number of impacts as a function of the direction of incidence of the bats, for the upper and lower halves of the rotor. The impact is maximum when flying against the wind (180 degrees), and is minimum when bats approach from approximately 45 degrees in the half below the hub, and when approaching from 315 degree (-45 degrees) in the half above the hub. The bats hit by the blades below hub height fall closer to the tower than those hit above the hub, as expected, and also are thrown in the direction of motion of the blades.

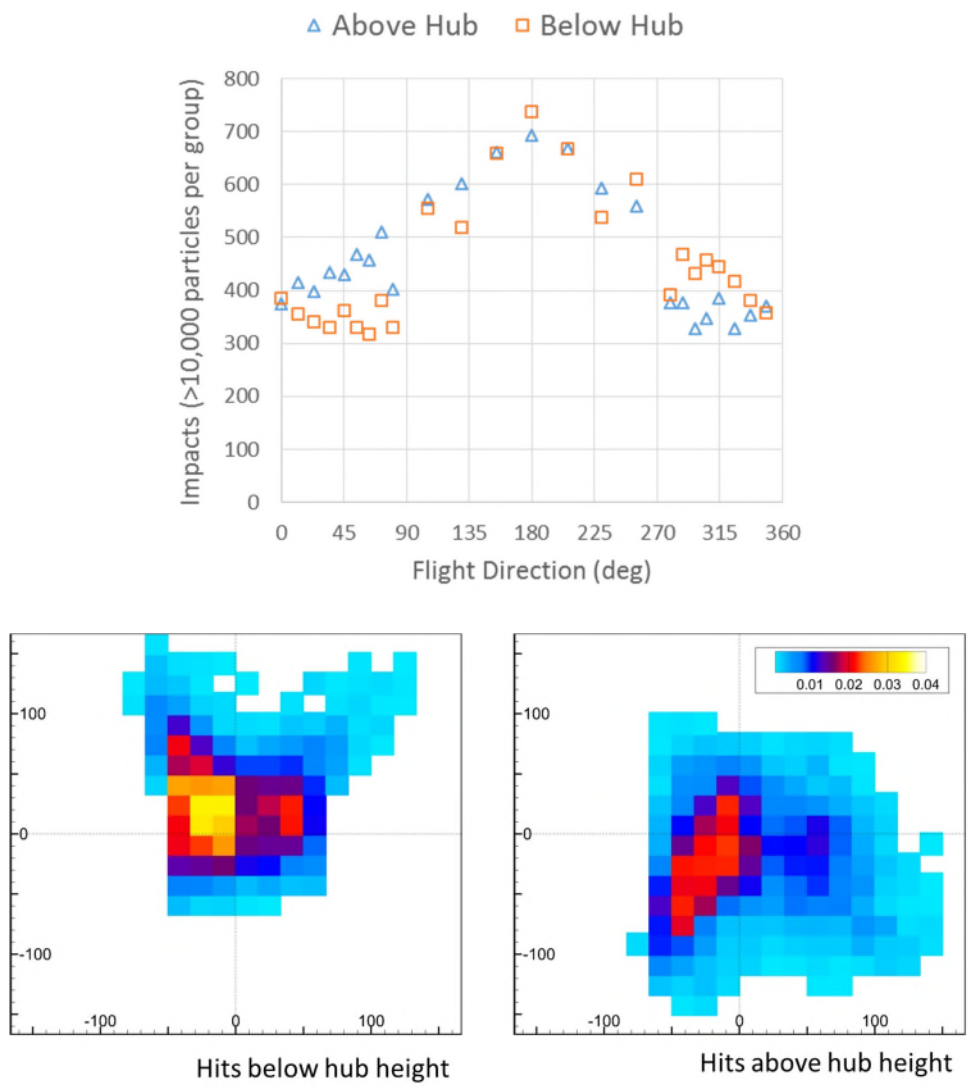

Figure 6-11 Impacts (top) and carcass distributions for bats hitting the rotor below hub height (bottom left) and above hub height (bottom right) for 28 g Hoary bats flying at 7 m/s relative to the wind.

6.6 Other Aerodynamic Effects

Results presented in previous sections highlighted the methodology and parametric dependence of the results on particles characteristics, such as mass, speed, restitution and drag coefficients. A second set of parameters, related to the aerodynamic problem were also studied to determine their relative importance on the results. Variables considered are incoming velocity profile, flow turbulence and turbine rotational speed. The effect of the different parameters was

studied separately. Turbulent fluctuations were considered only in conjunction with a non-uniform incoming profile.

6.6.1 Effects of Flow Variability.

In the previous section, uniform incoming flow quantities were used. This idealized situation is far from actual conditions in the field, characterized by intermittency (gusts) of the incoming wind, both in mean value as a whole and by localized temporal and spatial fluctuations typical of the atmospheric boundary layer (ABL). While this idealization might appear unrealistic, it is important to consider that the interaction time of the carcass, between blade and ground impacts, is relatively short compared to typical scales of the ABL and therefore using a uniform incoming velocity provides a reasonable estimate of the typical distribution to be found at a given mean wind speed.

The first effect considered is the inclusion of a dependence of the mean flow with the vertical coordinate. A standard logarithmic profile was chosen. This profile is fully determined using two parameters, such as roughness and free stream speed, or roughness and velocity at a given height. In our case, the velocity at hub height H was set to be equal to the required uniform velocity, and roughness height z_0 appropriate for cropland was used. The expression used is then

$$U(z) = U(H)\frac{\ln(z / z_0)}{\ln(H / z_0)} \tag{12}$$

The profile is shown in Figure 6-12. The variation is most important near the ground where the effect on falling particles is less important; for the region affected by the turbine, the profile is, within good approximation, linear. The changes in ground distribution of the particles are much less important that changes previously observed with other parameters, such as bat coefficients. Changes in distribution due to the mean velocity profile chosen, compared to results for uniform inlet velocity are shown in Figure 6-13 for a single set of particle parameters (u_p = 4.8 m/s; m = 8 g; C_D =0.4, e=0.2).

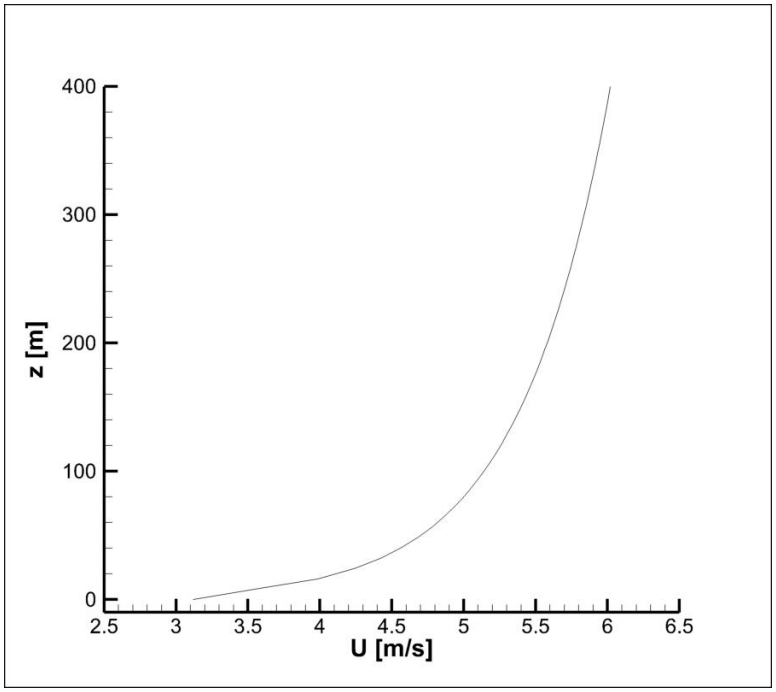

Figure 6-12 Incoming logarithmic velocity profile

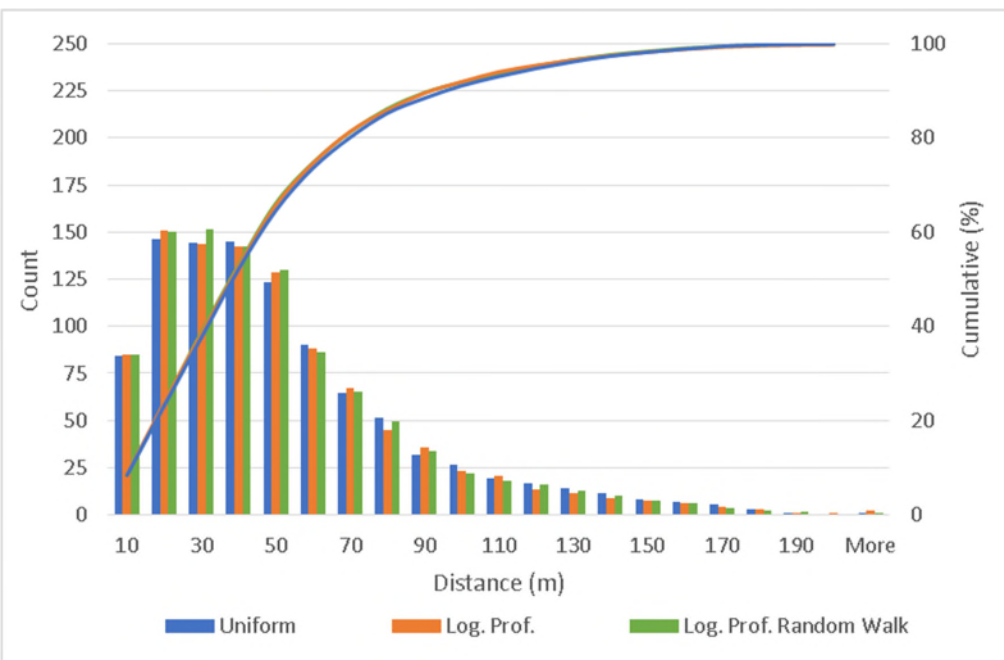

Figure 6-13 Histogram and cumulative as a function of the distance to the tower, for uniform incoming velocity (blue), logarithmic profile (orange) and logarithmic profile with random fluctuation superimposed to mean profile (green).

Figure 6-13 also shows a second improvement to the model, which is the simulation of fluctuations of the flow field due to turbulence. Different numerical models can be used to resolve the different scales of the flow field, with a corresponding increase in model complexity and computational requirements. The present model uses a Reynolds-averaged approach to turbulence modeling, which in practice means that only the mean and the lowest frequencies/larger amplitude fluctuations can be captured, while all other scales are represented by two turbulent scalar quantities, the turbulent kinetic energy (k) and the dissipation rate of k (ε). Figure 6-14 shows typical maps of these quantities for a simulation with a logarithmic profile inlet. Scaling estimates of velocity fluctuation u' and duration T_L can be obtained as:

$$u' = u - \bar{u} \sim \sqrt{\tfrac{2}{3}k} \tag{13}$$

$$T_L = 0.3\tfrac{k}{\varepsilon} \tag{14}$$

Figure 6-15 shows distribution of both the time scale and fluctuation level as percentage of the mean velocity. It is easy to see that effects are modest in the free stream, where fluctuations are small, and the time scale is fairly large. Regions of high turbulence, typically the wake have larger fluctuations, and smaller timescales.

Finally, as part of the particle tracking model, synthetic fluctuations are created based on this scaling. For this particular application a random distribution r_i = [0,1] is used to assign a fluctuation intensity and duration (τ_e) based on the particle location while integrating fluid forces on the particle:

$$\tau_s = T_L \log(r_i) \tag{15}$$

$$u' = (2r_i - 1)\sqrt{\tfrac{2}{3}k} \tag{16}$$

In the model, the fluctuation magnitude is maintained over as many time steps are necessary to reach the burst duration calculated; only then a new duration and magnitude are computed. Results shown in Figure 6-13 support the use of the simpler uniform inlet profile approach, as effects of turbulence are secondary to other uncertainty in the simulation.

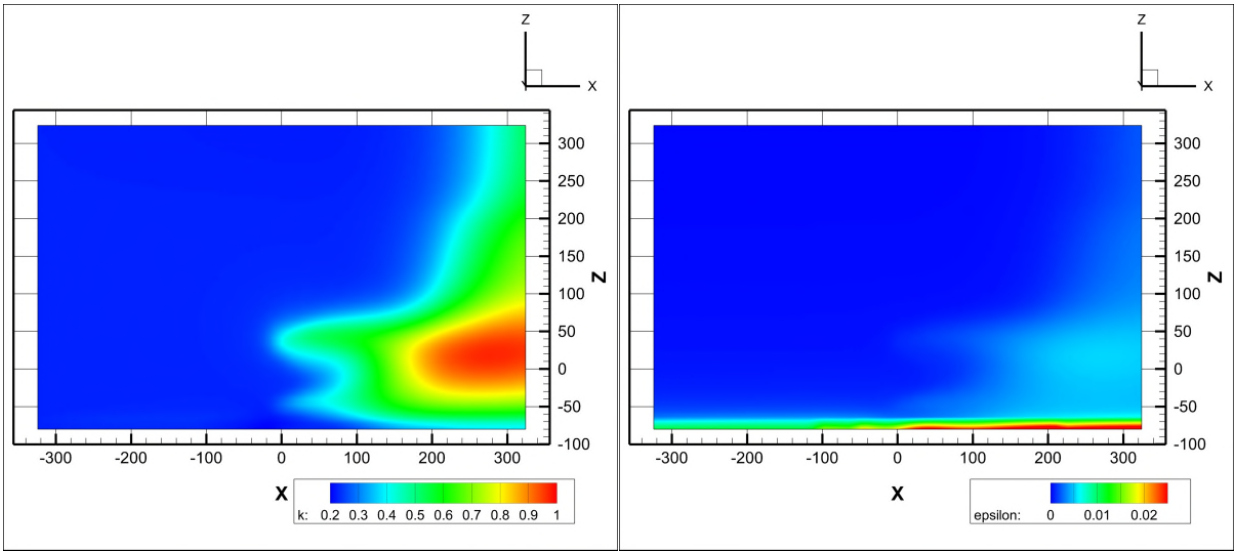

Figure 6-14 Turbulent kinetic energy (k, left) and dissipation rate (e, right) for logarithmic profile incoming velocity. Turbine rotor center is located at (x,z) = (0,0) in plots.

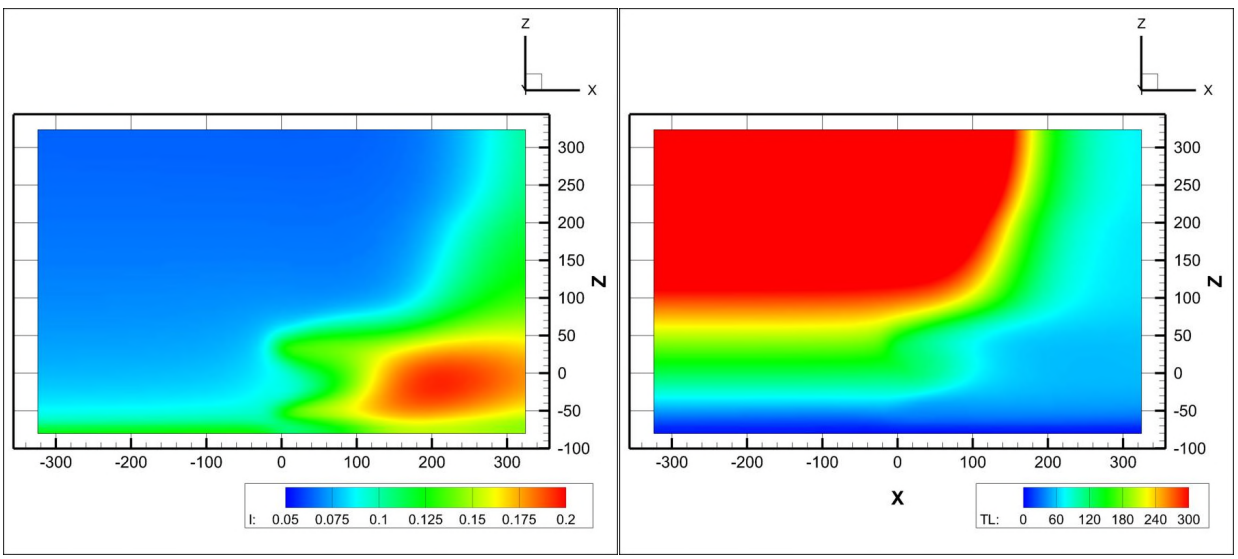

Figure 6-15 Fluctuation intensity as a function of the local velocity (left) and integral timescale (right) for logarithmic profile incoming velocity. Turbine rotor center is located at (x,z) = (0,0) in plots.

6.6.2 Effects of Turbine Rotational Speed

The final variable considered was the rotational speed of the turbine. As shown in Figure 6-1, wind turbines in the field do not strictly follow their power curve, but rather operate in a broader region, due to their limited ability to react to varying incoming wind conditions. From the

available SCADA data, the mean and standard deviation of the rotational speed were calculated for wind conditions around 5 m/s. The mean speed observed was 9.64 rpm, and the standard deviation 1.36 rpm. These values were used to simulate three representative turbine operations for low, mean and high rotational speed for the prescribed incoming wind. Figure 6-16 shows the results for the three cases. As expected, the higher the rotational speed, the further the carcasses are found, as their initial velocity, as imposed during impact with the blade is larger. The total number of bats impacted also increases slightly.

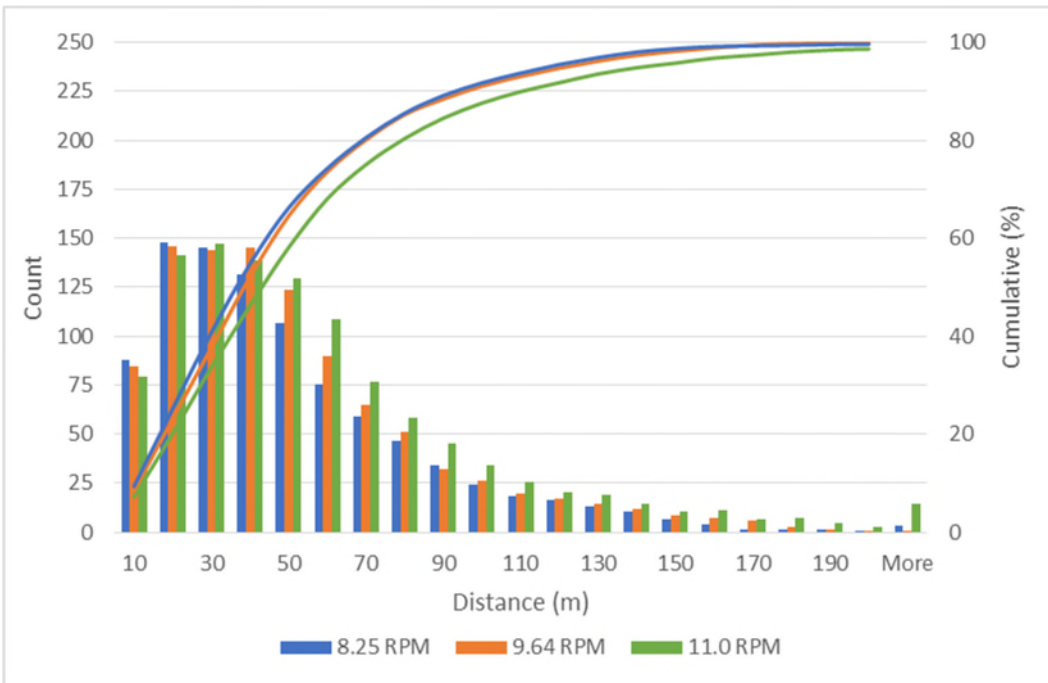

Figure 6-16 Histogram and cumulative as a function of the distance to the tower, for 8.25 RPM (blue), 9.64 RPM (orange) and 11.0 RPM (green).

7 COMPARISON AGAINST FIELD DATA

Data from two field survey campaigns (2015 and 2016) were available for comparison to simulations. For the first campaign only access roads and clear areas around the turbine (pads) were surveyed. The second campaign added square plots around turbines for selected locations. Two sizes of plots were considered, one 60 m on the side, and the other with 200 m.

7.1 2015 Survey

In 2015 bat carcass surveys were conducted around 99 turbines at Lundgren and 47 turbines at Macksburg wind farms (92% of the total number of turbines), operated in Iowa by MEC. Carcass surveys were conducted at access roads and pads around the turbines to a distance of approximately 100 m for both wind farms. For Lundgren, bat carcass surveys started on 14th April 2015 and ended on 26th October 2015. For Macksburg, the survey started on 11th May 2015 and finished on 13th October 2015. The survey frequency at individual turbines was generally between 1-8 days at both wind farms. The cumulative carcass count was 290 for Lundgren and 140 for Macksburg for the survey period. The majority of bat species found in 2015 include Eastern Red bats, Hoary bats, Little Brown bats and Silver Haired bats.

Figure 7-1 shows the radial distribution along with the cumulative histogram displaying the number of bat carcasses for turbines searched at Lundgren and Macksburg wind farms. Most of the bat carcasses fall within 100 m of the turbine tower. There are few instances of bat carcasses falling beyond 80 m from the tower, and include Hoary, Eastern Red and Little Brown Bats. Some of the carcasses were reported as having been scavenged and some of them were found to be intact. About 50% of the bat carcasses were found within a distance of 10 m.

The spatial distribution of bat carcasses is shown in Figure 7-2, with (0,0) located at the turbine tower. There is a clear pattern of carcasses found along the access roads, which corresponds to the North-South and East-West axes in Lundgren.

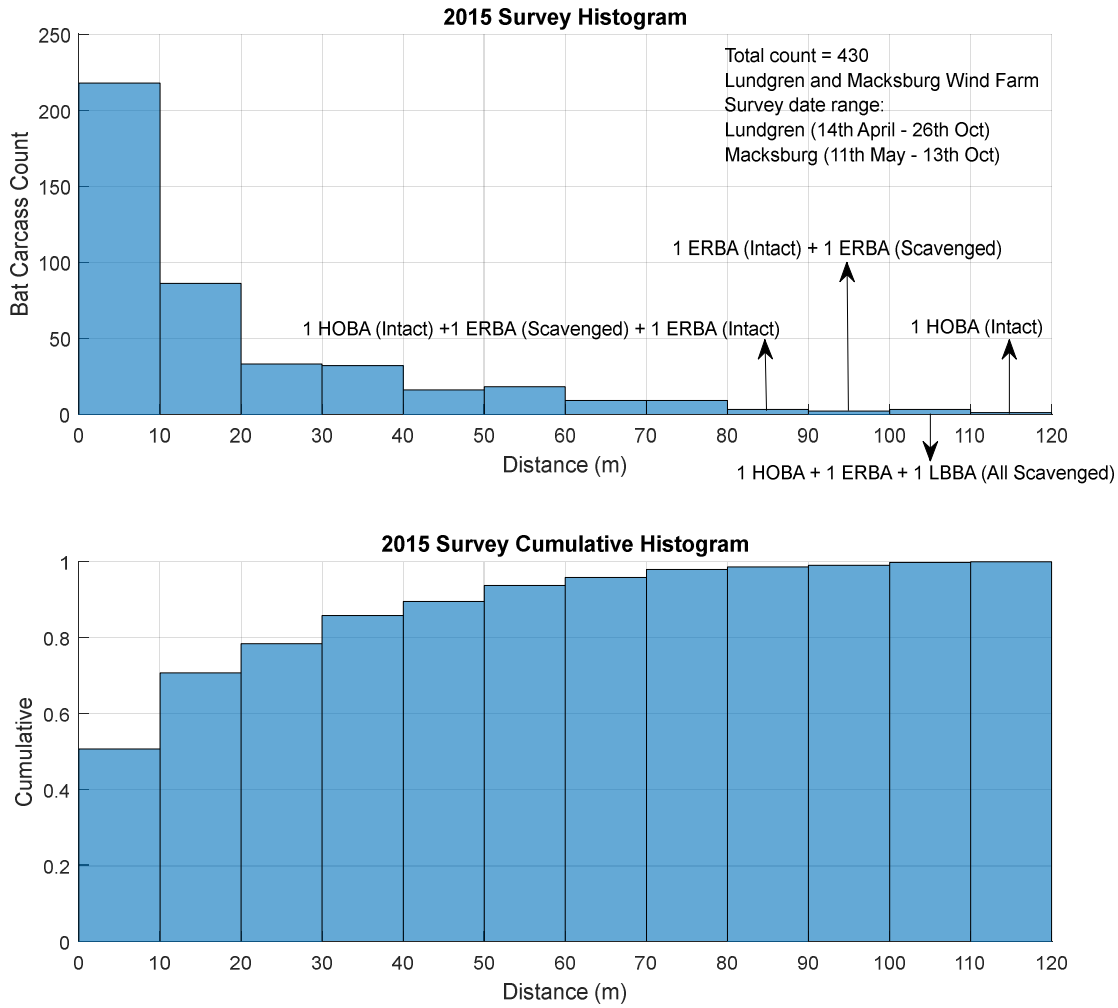

Figure 7-1 Histogram (top) and cumulative (bottom) as a function of the distance to the tower for all bat species at Lundgren and Macksburg wind farms for the 2015 survey.

Data from the numerical model shown in Figure 6-10 was used to correct the survey data from Lundgren from a limited search area (pads plus access roads) to a full circular search area within a 100 m radius from the tower. The radius of the pad and width of the access road were estimated for a typical Lundgren turbine, shown in Figure 7-3 from Google Maps. The correction performed considers that the number of carcasses found within a distance r and $(r+\Delta r)$ from the tower is proportional to the ratio between the circumferential area $2\pi r \Delta r$ and the local searched area, with

the search area computed as $2\pi r\Delta r$ within the pad and $5\Delta r$ along the access road. In this study, $\Delta r = 2$ m was adopted for the integration. Since the original number of bats injected in the simulation was arbitrary, the number of bats impacted was scaled so the total number found in the access road matches the 292 bats found in Lundgren.

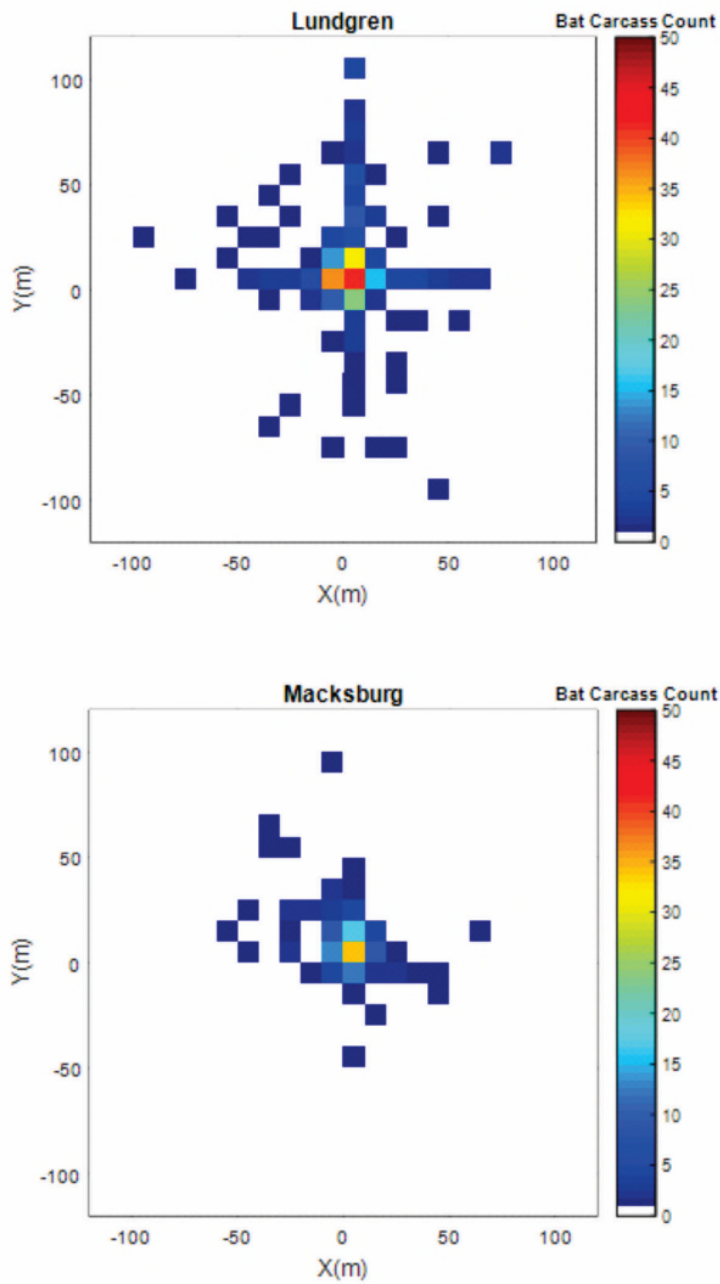

Figure 7-2 Spatial distribution of all bat carcasses found in surveys conducted at Lundgren and Macksburg wind farms in 2015.

Figure 7-3 Typical Lundgren pad and access road.

Histograms showing survey and model results are shown in Figure 7-4 and Figure 7-5 . Figure 7-4 shows the number of bats found in the pad and access road, while Figure 7-5 shows the total number of bat carcasses that should have been found if the search area had covered the whole circular area with the same collection efficiency.

The correction procedure concludes that a full search would have found 7107 carcasses at Lundgren, of which 292 fell within the pad and access road. The model predicts 6976 bats total, of which 292 fall in the search area. Same comparison shows 140 bats for the search area at Macksburg, for both data and model and a corrected value of 1942 carcasses, compared to a predicted value of 3346. It is important to note that there is significant uncertainty with bats falling farther out from the turbine, where the correction factor is very large. Different bat species and behavioral assumptions will likely change results considerably.

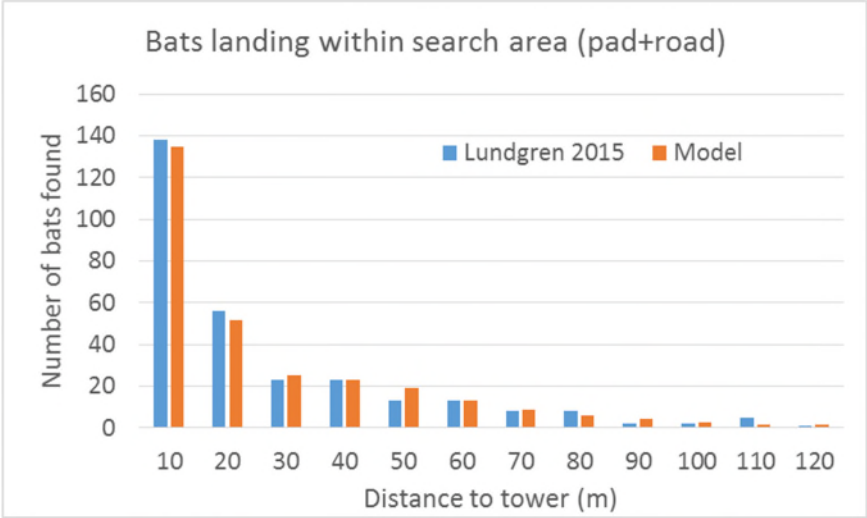

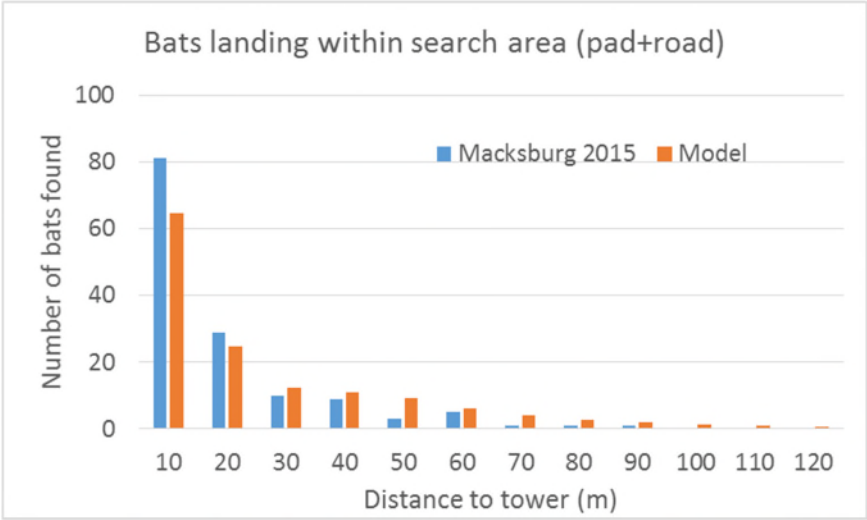

Figure 7-4 Measured and predicted histograms for the search area (pad+road) for Lundgren (top) and Macksburg (bottom) for 2015 survey.

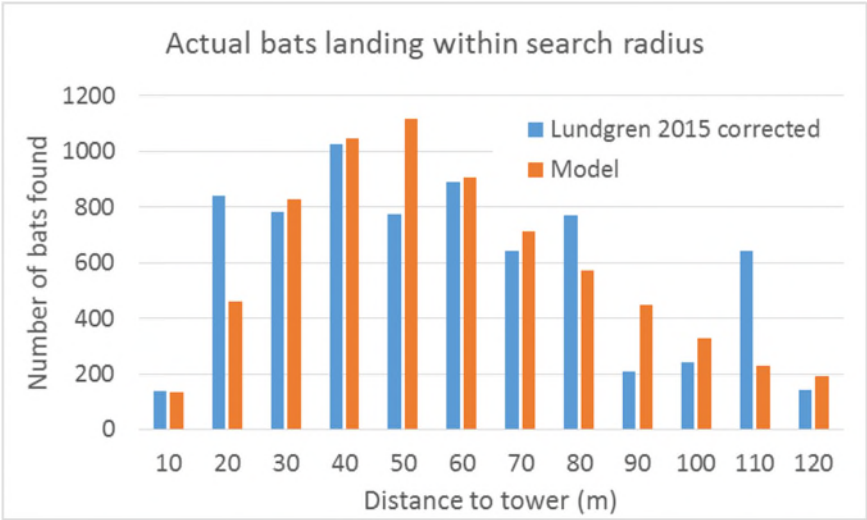

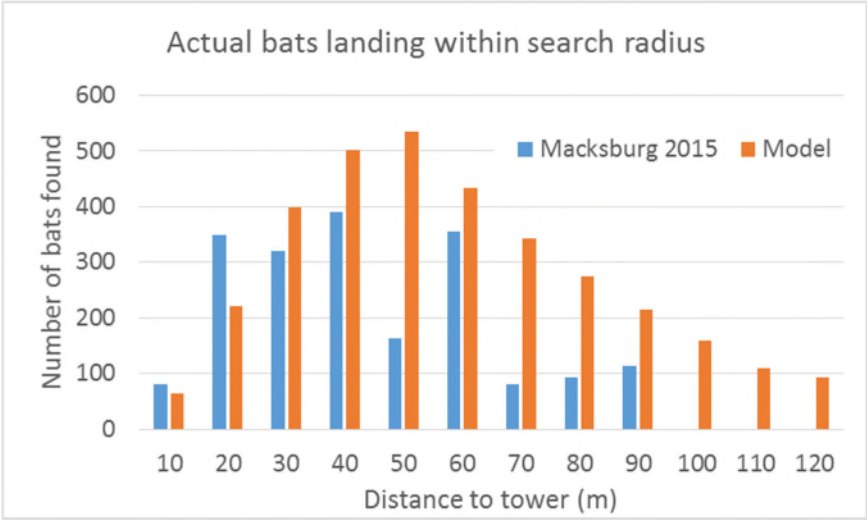

Figure 7-5 Measured and predicted histograms for the total circumferential area for Lundgren (top) and Macksburg data (bottom) for 2015 survey.

7.2 2016 Survey

In 2016, bat carcass surveys were conducted at all wind turbines at Lundgren (107 turbines) and Macksburg (51 turbines), operated in Iowa by MEC. For surveying, turbines at the two wind farms were divided into four groups: road/pad-only searches, and searches in cleared square plots of sizes 60 × 60 m, 100 × 100 m and 200 × 200 m, respectively. Table 7-1 shows the number of turbines in each group.

Table 7-1 Total Number of Turbines in each Group

Facility	60 × 60 m	100 × 100 m	200 × 200 m	Road/Pad	# turbines
Lundgren	11	0	10	86	107
Macksburg	0	0	10	41	51

The survey started on 15th July 2016 and ended on 14th November 2016. The cumulative carcass count was 254 at Lundgren and 129 at Macksburg during the survey period. The majority of bat species found in 2016 include Hoary, Eastern Red, Evening and Big Brown Bats. Figure 7-6 and Figure 7-7 show radial distributions and cumulative histograms for Lundgren and Macksburg farms for searches at road/pads and cleared square plots, respectively. Four bat carcasses were found at distances greater than 80 m for the turbines that were searched for road and pads, two Eastern Red Bats, one Hoary Bat and one unidentified. The Hoary Bat and one Eastern Red Bat were reported as scavenged while the other Eastern Red Bats was intact. It is important to notice that both Hoary Bat (Heavy species, high C_d) as well as Eastern Red Bat (light species, low C_d) show up in the tail of the distribution as was the case in 2015. For square plots (Figure 7-7), bat carcass were found no farther than 80 m from the tower.

Figure 7-8 compares the cumulative distribution function (CDF) for road/pad and square plots searches. The percentage of bat carcasses landing within 10 m from the tower for the road/pad and square searches is 65% and 42%, respectively. It is interesting that the number of bat carcasses found in the first 40 m from the tower was larger for road and pads than for squared plots searches.

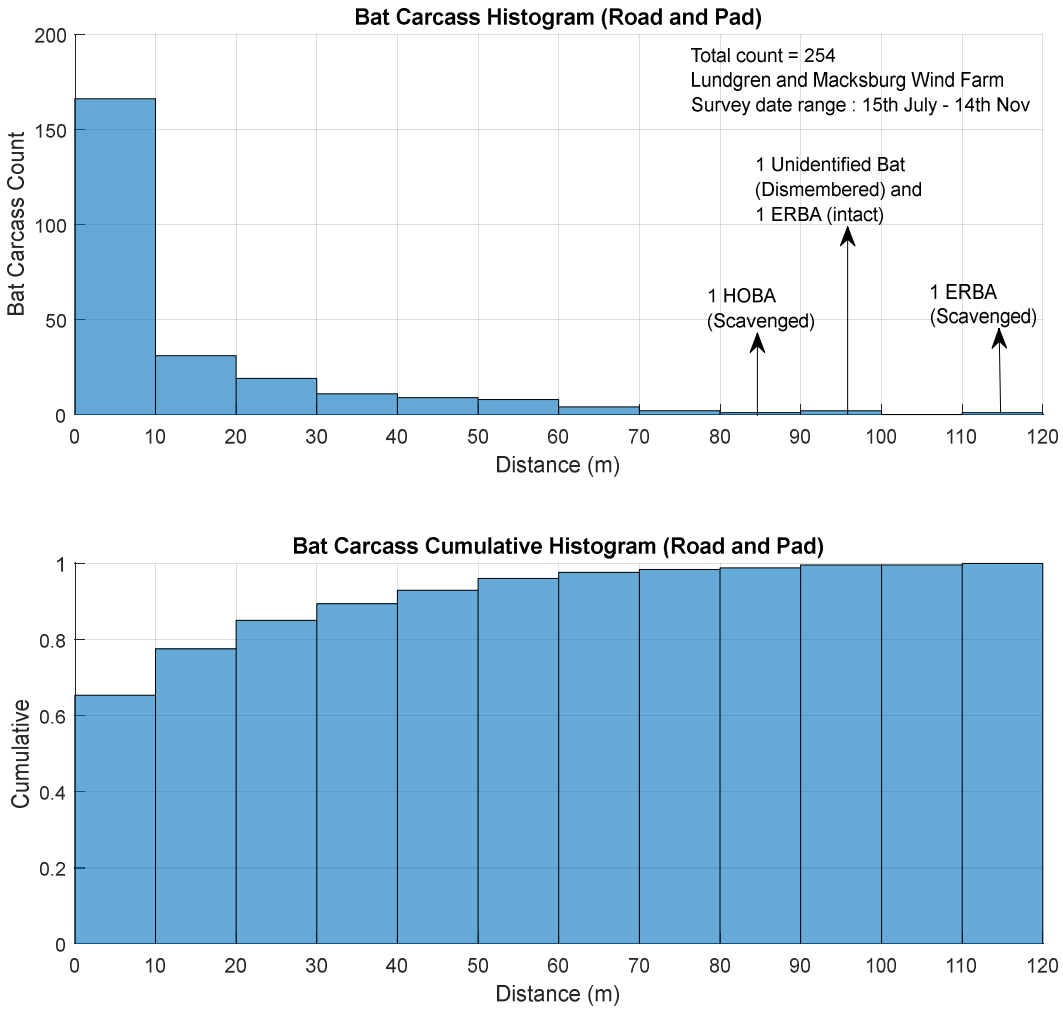

Figure 7-6 Histogram (top) and cumulative (bottom) as a function of the distance to the tower for all bat species at roads/pads in Lundgren and Macksburg wind farms for 2016 survey.

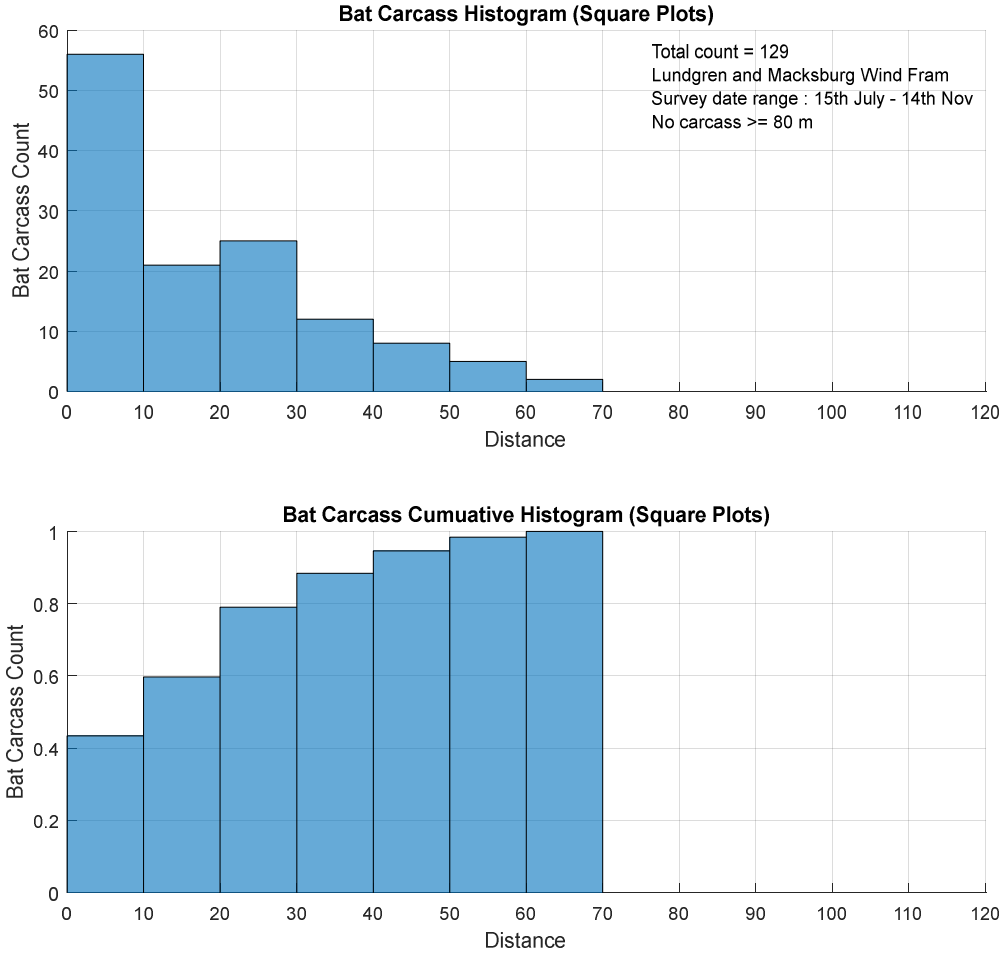

Figure 7-7 Histogram (top) and cumulative (bottom) as a function of the distance to the tower for all bat species at square plots in Lundgren and Macksburg wind farms for 2016 survey.

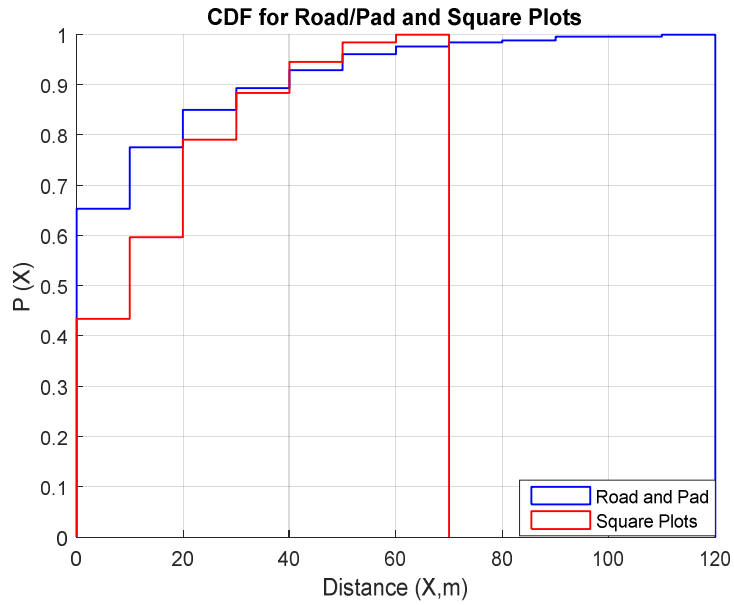

Figure 7-8 CDF comparison between Road/Pad and Square plots

7.3 2015 and 2016 Survey Data Comparison

Figure 7-9 and Figure 7-10 show the CDF and spatial carcass distribution in the 2015 and 2016 surveys along roads and pads. As expected, the carcass distribution in both surveys is similar, but in 2016 more carcasses were found in the immediate vicinity of the turbine. This similarity builds confidence in the field data collected from roads and pads.

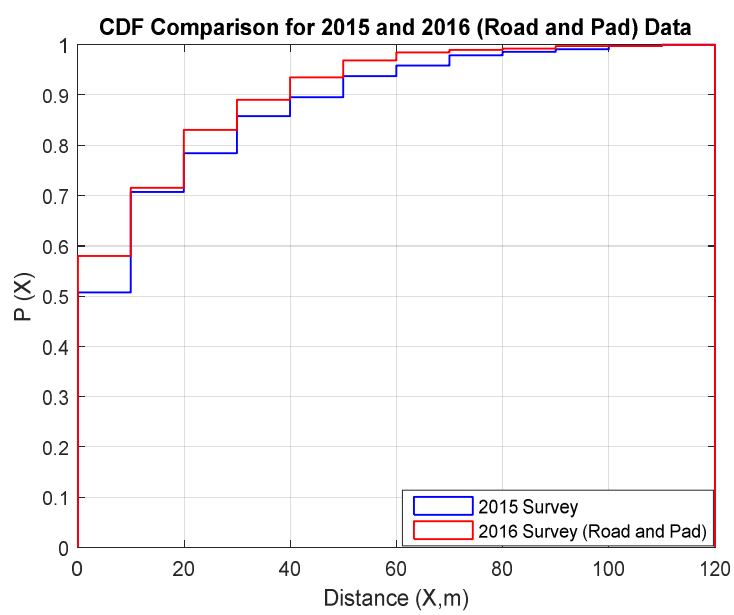

Figure 7-9 CDF comparison between 2015 and 2016 surveys

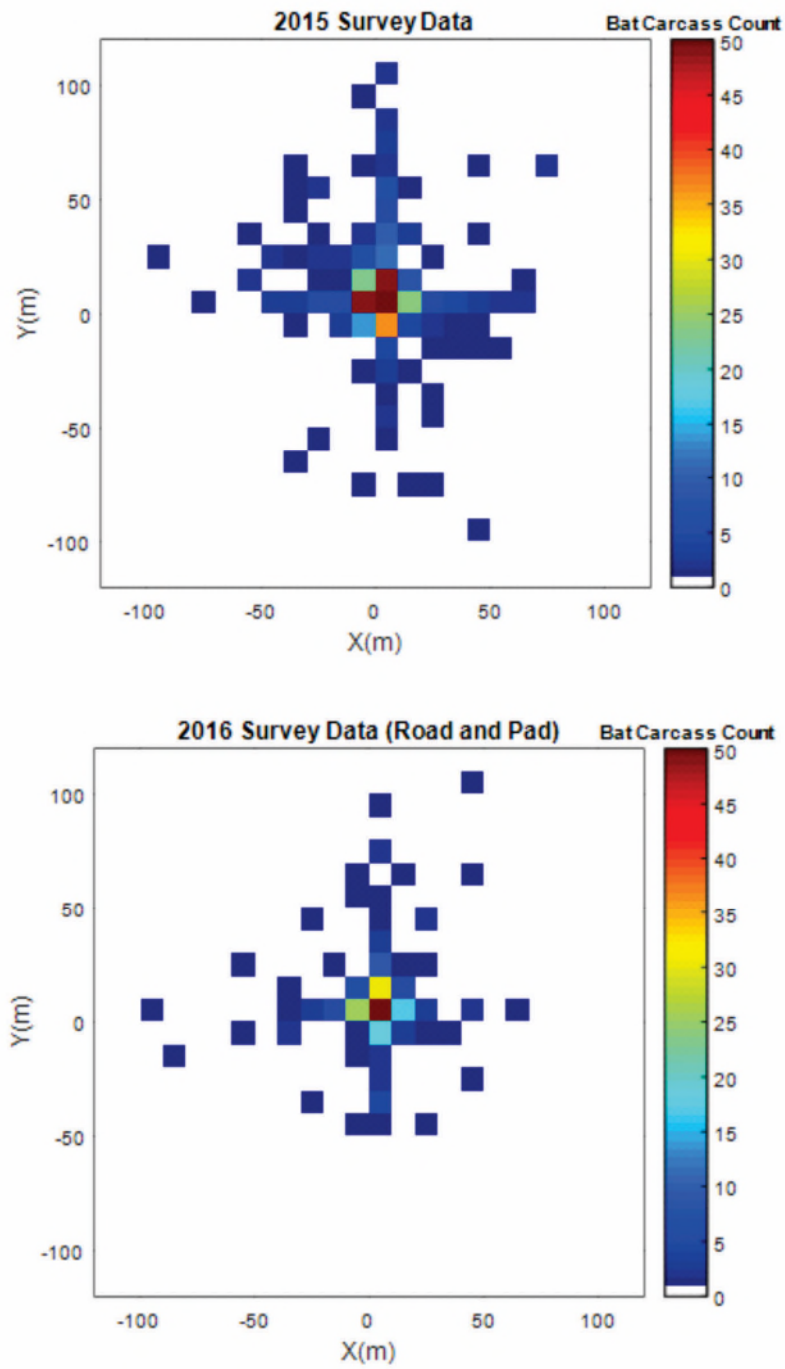

Figure 7-10 Carcass distribution in 2015 (top) and 2016 (bottom) surveys

7.4 Comparison of Survey Data with Simulation Results

129 carcasses (about 33% of the total) were found for turbines with survey plots, however a significant number of those carcasses were recovered from locations close to the tower where conditions are likely similar to those for turbines where the search area was only pad and road. Data provided shows that half of the carcasses from the 200m × 200m plots from Lundgren would not have been found using a 60m × 60m plot, but only 10% (6 out of 60) would not have been found with the smaller plot at Macksburg. The total number of carcasses in the extended area from 60m × 60m to 200m × 200m is 20, or 15% of the carcasses from turbines with search plots. Therefore, data from the two types of survey plots are combined to improve the quality of the dataset, which is fully valid up to a radius of 42m, and has higher uncertainty, due to the reduced number of turbines sampled, for larger radii.

Data for turbines in the roads and pads only subset were analyzed first. Following the same procedure described for the 2015 survey, Figure 7-11 through Figure 7-12 show respectively the radial distributions for the raw data and comparison to modeled data for each wind farm. As it was detailed for the 2015 survey analysis, the simulations were scaled to have the same number of carcasses found on the search areas surveyed. The corrected data, following the procedure detailed previously, shows a much better agreement between model and data for Lundgren than for Macksburg, but overall worse agreement than for 2015. The model over predicts the number of carcasses found by 30% for Lundgren (2840 to 3770), yet still predicts correctly that the peak distribution occurs at a distance of about 50 m. The prediction from Macksburg is about 2.5 times larger than the corrected field data (853 to 2292). No clear peak in the distribution is observed. In both cases the model over predicts the quantity of carcasses at larger radii, contributing to the larger differences observed compared to 2015. This is not surprising as the distributions from 2016 are heavily shifted towards smaller radii. Compared to the data from 2015, a larger number of bats were found near the turbine: for 2015, 48% and 58% of the carcasses were found within 10 m of the tower, while that quantity is 61% and 71% for 2016 for Lundgren and Macksburg, respectively. The ratio for the model data is 46% (these quantities referred to the search area of pads and roads). These differences can be attributed to a large number of variables, including differences in wind speed conditions and bat properties, as well as changes in search efficiency. Unfortunately the available data cannot provide a definite answer to explain such differences due to the low number of bats found further away from the turbine towers and the resulting poor statistics. In general the

parameters used in the simulation (considering both aerodynamics conditions, as well as particles parameters) appear more appropriate to conditions at the Lundgren wind farm.

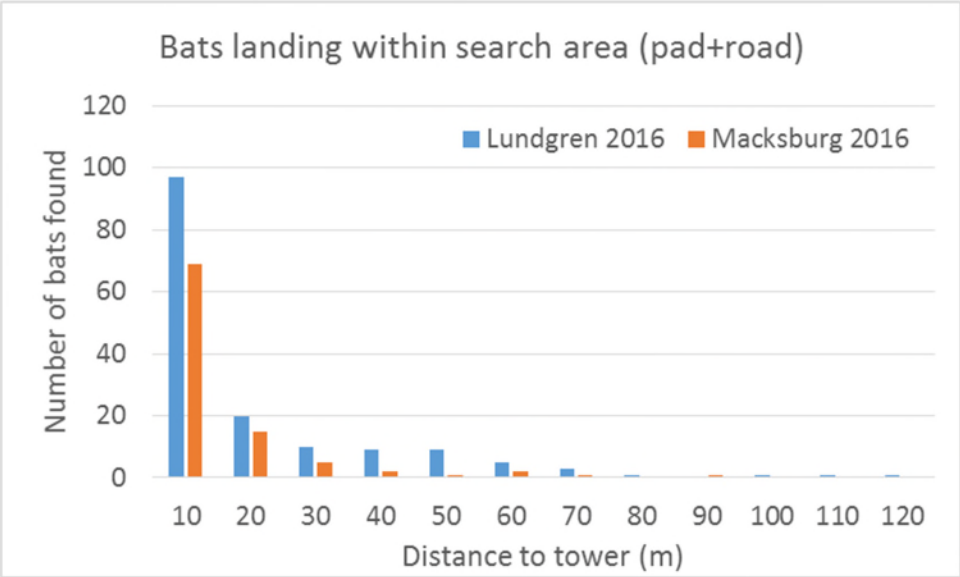

Figure 7-11 Lundgren and Macksburg data for 2016 campaign (pad and road turbines only).

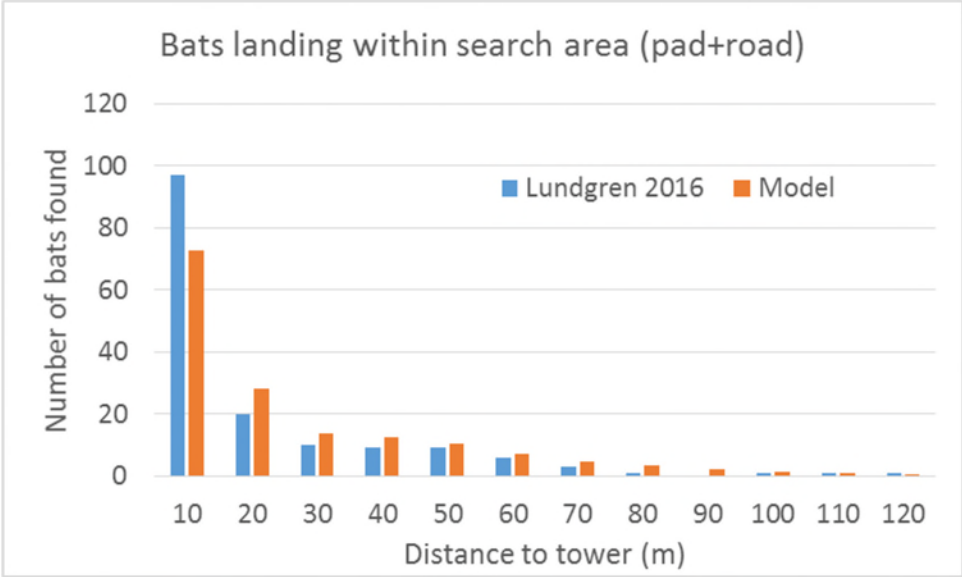

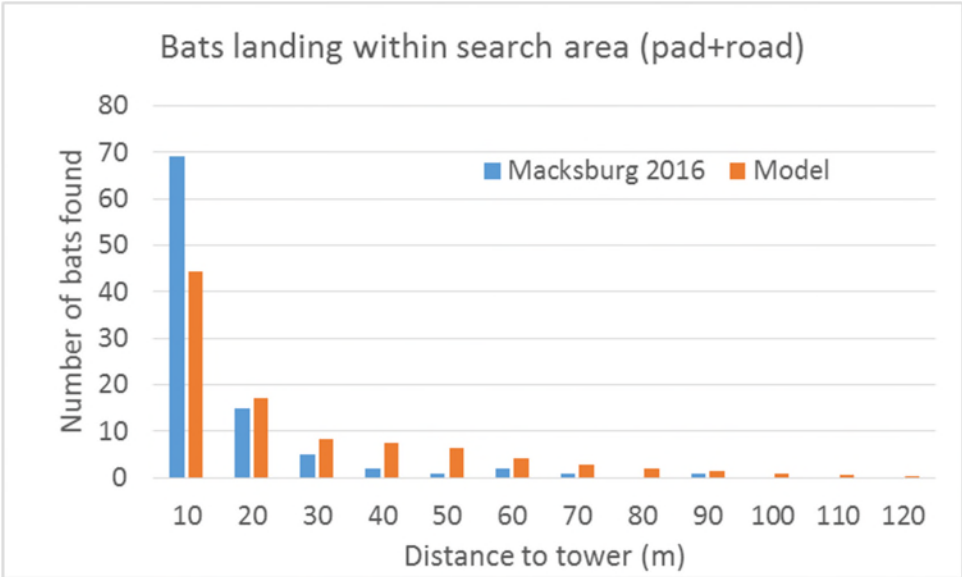

Figure 7-12 Measured and predicted radial distributions at pads and roads for Lundgren (top) and Macksburg (bottom) for 2016 survey.

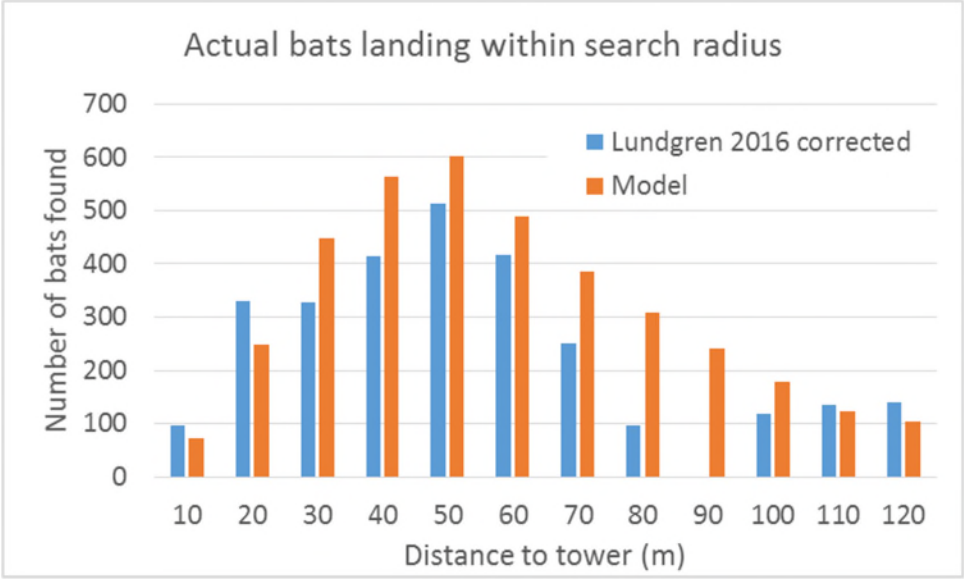

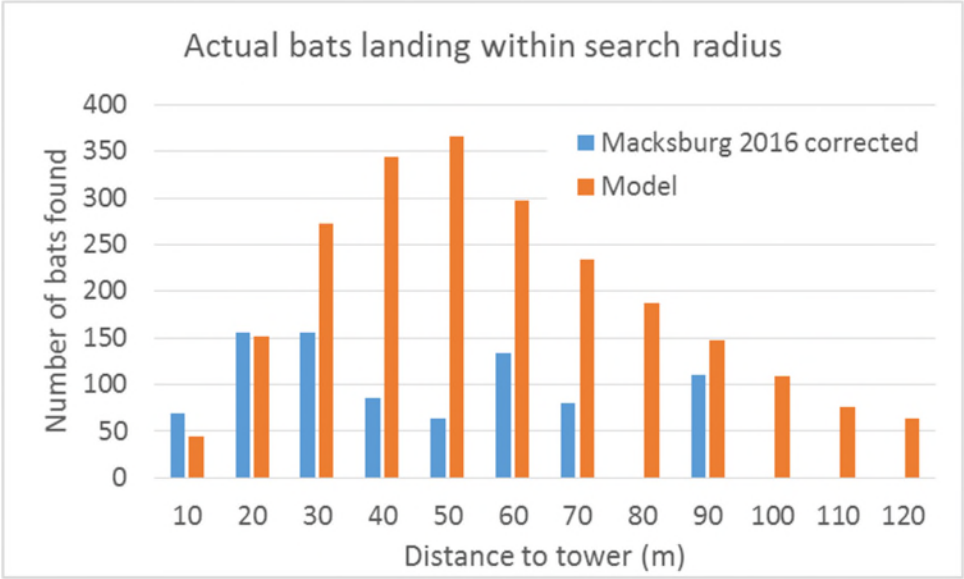

Figure 7-13 Histograms for the total circumferential area including corrected Lundgren data (top), Macksburg data (bottom) and model predictions for each case, for 2016 survey.

The 2016 campaign also includes data over the complete area surrounding the turbines up to 30 to 100 meters away from the tower. The data has the advantage of not requiring correction for areas not searched, as needed for data from access roads, but has a considerably smaller search efficiency than the roads and pads have. Comparing the circumferential data to model results requires assumptions regarding the search efficiency that were not considered for roads and pads (unit efficiency was consider for those cases). A possible way to estimate the search efficiency is

to consider that all turbine searches have similar efficiency near the tower (in the turbine tower pad). Figure 7-14 compares the distribution of carcasses up to 10 m from the tower. The values from the "Pad and roads" group only have been scaled down to have the same total number of carcasses as the "Square plots" group. The scaling factor used is 3.05, as 174 carcasses were found in the first group and 57 in the second. Another possible scaling, independent of the carcasses found would be simply to divide by the number of turbines in each group. That factor would be about 3.5 which is roughly comparable with the one used.

Using this scaling factor, geometrically corrected values for "Pad and Roads" turbine group can be compared to "Square plots" data. The result of the comparison is shown in Figure 7-15. The ratio of the number of carcasses found for each distance gives an estimate of the relative search efficiency for square plots compared to access roads (Figure 7-16). Values found vary from about 40% close to the tower (r<30m) to about 10% for larger distances. These results are similar to estimates of relative searcher efficiency from the field. Based on the uncertainty of the actual search efficiencies for the search plots, and the relatively small number of carcasses found compared to those on access roads, no further comparison is done to model quantities based on these data.

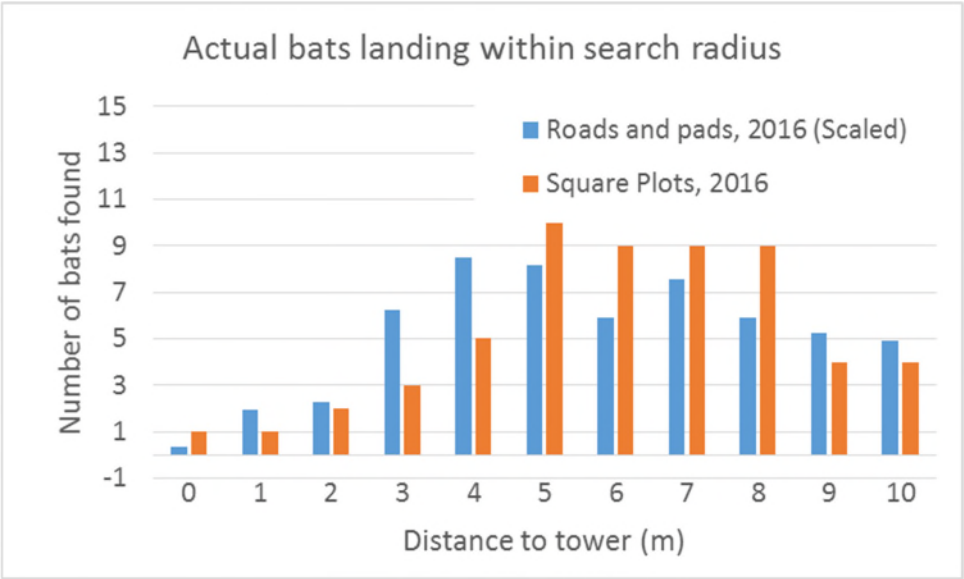

Figure 7-14 Combined Lundgren and Macksburg data for 2016 campaign near the turbine tower. "Pad and access road" turbine group data have been scaled by a factor of 3.05 for comparison to data from "Square plots" turbine group.

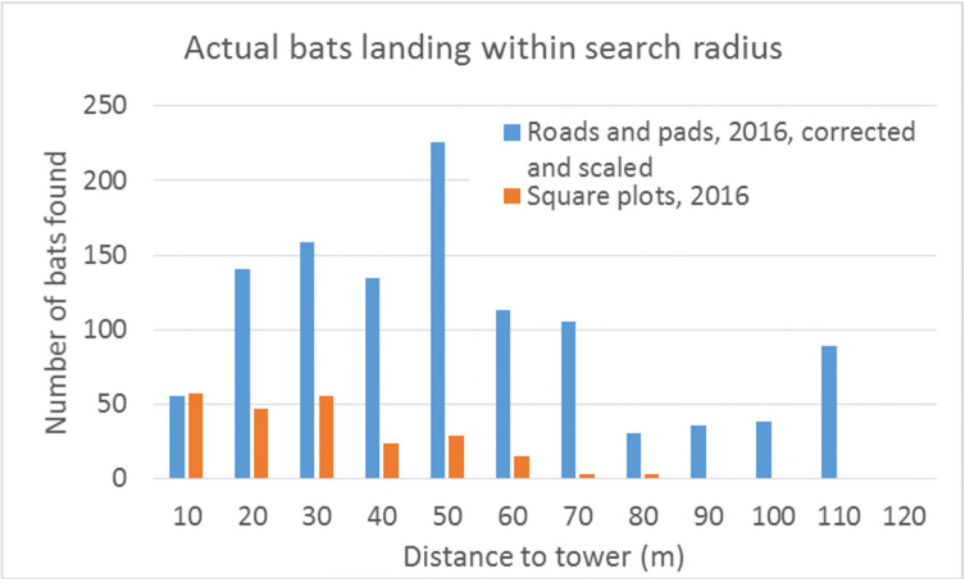

Figure 7-15 Combined Lundgren and Macksburg data for 2016 campaign (all distances). "Pad and access road" turbine group data have been geometrically corrected, and scaled by a factor of 3.05 for comparison to data from "Square plots" turbine group.

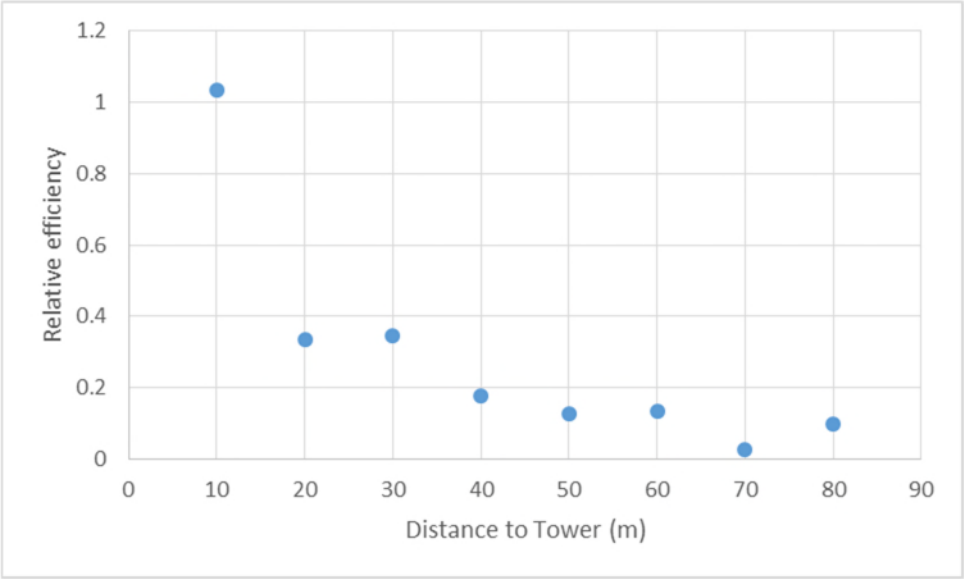

Figure 7-16 Combined Lundgren and Macksburg data for 2016 campaign Relative search efficiency between "Pad and access road" turbine group (geometrically corrected and scaled by a factor of 3.05 for comparison) to "Square plots" turbine group.

8 CONCLUSIONS AND FUTURE WORK

Summary results from simulations using the CFD-Lagrangian modeling approach for typical conditions when bats may be impacted by wind turbines are as follows:

- For all the simulation cases discussed above, 90% of the bats fall within 100 m of turbine tower.
- Bats flying faster have lower probability of being struck by a wind turbine, and their carcasses distributed more closely around the turbine.
- Heavier bat carcasses are concentrated closer to the turbine compared to the lighter ones.
- Lower values of carcass drag coefficient and higher restitution coefficient values results in more extensive carcass distributions.
- Flying against the wind, approaching the turbine from behind, greatly increases the probability of impact and in distributions covering a larger area.
- Bats hit on the lower half of the rotor fall closer to the tower than those hit on the upper half.

Assumptions were made regarding various parameters in the bat model and in the context of movement of bats approaching the turbine. Additional effort should focus on refining the assumptions to develop a robust model that can reliably generate the spatial distribution of bat carcasses for different turbine features, bat physical and behavioral characteristics, as well as varying meteorological conditions.

The drag (C_d) and restitution (e) coefficients were assumed constant for each species, as obtained from the field data presented in Section 5. This is an approximation since it is known that the drag coefficient will depend on size and speed of the bat. If available, a wider sample of bats could be used to determine more accurate values to use in the future.

Turbulence was added in the CFD model and one condition was tested. While the effects observed were secondary to other parameters, turbulence may still affect the behavior of bat flight, impact probability, and may affect the fall distribution of bat carcasses. Turbulence also adds a random motion characteristic to the bat flight, as has been reported in the field. The simulated conditions considered fairly low levels of incoming turbulence, and actual field conditions can

occur with stronger levels. However, at this point, turbulent effects are not considered as critical as other uncertainties in the model.

Wind turbine blade rotational speed was shown to have a more significant effect on carcass distribution. At the current level of effort, using a constant rotational speed and steady wind is appropriate; however combining field data regarding wind and operational conditions, likely to have been prevalent during bat impact, will require the simulation of more conditions to better assess the probable conditions during impact and the consequences in carcass distributions. Ideally, a full range of wind velocity and rotational speed conditions would be simulated to generate results that could be used to better determine probabilities of carcasses location, which would allow for a better comparison against specific field conditions.

A uniform distribution of bats was assumed to approach the turbine. Different bat species exhibit different behavior and migrate at different preferential altitudes. Implementing migration altitude information in the bat model will result in bats striking the rotor above the hub or below the hub, which may further change the carcass distribution predictions.

Regardless of the simple approximations used for the bat properties and the lack of behavioral models (other than the well documented ability to avoid static objects) and turbulence, the model performed remarkably well when compared with data from the 2015 and 2016 surveys at Lundgren, a fairly well when compared to Macksburg data. Figure 7-3 shows that distribution of points at Lundgren (due to the location of access road at this facility) covers the different regions around the turbine better than at Macksburg, which can explain the better agreement with the model. Full search of the area around the turbine produced much lower numbers than expected, and the comparison of the model with this data was less useful than comparisons with data from access roads.

Given the low search efficiency in plots, the possible correlation between geometrical distribution of data in the two wind farms and their match to model conditions, and general remaining questions regarding azimuthal distribution (anisotropy), it is recommended that if further field campaigns were considered, strips of high visibility material similar to those for the access road are used around selected turbines (in patterns of 4 or 8 rays) to conclusively determine angular distributions around a turbine that can be better correlated to wind conditions and turbine operation. While such arrangement will have a setup cost, it would greatly reduce the time required to search, as well as increase the search success rate.

Future work can be focused on two areas. The first is using the model to correct limited area field data and compute total mortality rates. This will require tuning the parameters to specific prevalent wind and operational conditions to properly predict the spatial distribution of the carcasses and allow the model to extrapolate field data limited, for instance, to roads and pads.

The second area is to add behavioral models, based on observations and field data, to improve the model to a predictive impact model. Such a model would be able to predict what is the probability of a bat flying near the turbine to be hit by a blade, and can thus be used to evaluate mitigation measures.

9 REFERENCES

1. Altringham, John D. 1996. *Bats Biology and Behavior*. New York: Oxford University and Press.
2. Arnett, E.B. 2005. *Relationships between bats and wind turbines in Pennysylvania and west Virginia: an assessment of fatality search protocols, patterns of fatality and behavioral interactions with wind turbines*, final report for Bats and Wind Energy Cooperative, by Bat Conservation International, Austin, Texas, USA.
3. Arnett, E. B., Schirmacher, M., Huso, M. M. P. and Hayes, J. P. 2009. *Effectiveness of changing wind turbine cut-in speed to reduce bat mortalities at wind facilities*. An annual report submitted to the Bats and Wind Energy Cooperative. Bat Conservation International. Austin, Texas, USA.
4. AusWind 2005. *Wind farms and birds: interim standards for risk assessment*, Report no. 2003. 35 (2.2), Australian Wind Energy Association, Carlton North, Victoria.
5. Baerwald, E. F., D'Amours G. H., Klug, B. J. and Barclay R. M .R. 2008. *Barotrauma is a significant cause of bat fatalities at wind turbines*. Curr Biol 18:695–696GAO (Government Accountability Office). 2005. Wind Power: Impacts on wildlife and government responsibilities for regulating development and protecting wildlife. GAO- 05-9006. Washington, DC.
6. Baker, R. 1983. *Michigan Mammals*. Lansing, Michigan, USA: Michigan State University Press.

7. Barbour, R. and Davis, W. 1974. *Mammals of Kentucky*. Kentucky: The University Press of Kentucky.

8. Biological Opinion: *Application for Incidental Take Permit and Habitat Conservation Plan*, Criterion Private Partners, LLC for the Criterion Wild Project, Garrett County Maryland, USFWS, January 2014.

9. Burgin, L. V., Edelsten, L. and Aspden, R. M. 2014. *The mechanical and material properties of elderly human articular cartilage subject to impact and slow loading*. Med Eng Phy, 36 (2), 226:32.

10. Carceres, C. and Barclay, R. 2000. *Myotis Septentrionalis*. Mammalian Species, 634: 1-4.

11. Churchfield, M., Lee, S. and Moriarty, P. 2012a. *Overview of the Simulator for Wind Farm Application (SOWFA)*. NREL technical report. Accessible at: https://nwtc.nrel.gov/system/files/SOWFA_tutorial_05-20-2014.pdf.

12. Churchfield, M. J., Lee, S., Michalakes, J., and Moriarty, P. J. 2012b. *A numerical study of the effects of atmospheric and wake turbulence on wind turbine dynamics*. Journal of Turbulence. 13(14):1.

13. Clift, R., Grace, J. R. and Weber, M. E. 1978, *Bubbles, Drops and Particles*, Academic Press INC, 111 Fifth Avenue, New York, New York 10003.

14. Cryan, P. M. et al. 2014. *Behavior of Bats at Wind Turbines*, Proc Natl Acad Sci.

15. Cryan, P. M. and Brown, A. C. 2007. *Migration of bats past a remote island offers clues toward the problem of bat fatalities at wind turbines*, j.biocon. 2007.05.019.

16. Coburn, L., Cerone, L., Torney, C., Couzin, I. D. and Neufeld, Z. 2013. *Tactile interactions lead to coherent motion and enhanced chemotaxis of migrating cells*. Phys Biol., 10 (4): 046002.

17. Erickson, W. P., Jeffery, J. Kronner, K. and Bay, K. 2004. *Stateline wind project wildlife monitoring report*: July 2001-December 2003, report for FPL Energy, Stateline Technical Advisory Committee, Oregon Department of Energy, by Western EcoSystems Technology Inc., Cheyenne, Wyoming and Walla Walla, Washington & Northwest Wildlife Consultants Inc., Pendleton, Oregon, USA.

18. Fenton, M. and Barclay, R. 1980. *Myotis Lucifugus*. Mammalian Species, 142:1-8.

19. Fugita, M. and Kunz, T. 1984. *Pipistrellus Subflavus*. Mammalian Species, 228:1-6.

20. Gauthreaux, S. A. 1996. *Suggested practices for monitoring bird populations, movements and mortality in Wind Resource Areas*. in Proceedings of National Avian-Wind Power Planning Meeting II. Palm Springs, California, 20-22 September 1995, prepared for the Avian Subcommittee of the National Wind Coordination Committee by RESOLVE Inc, Washington DC.

21. Goehring, H. 1972. *Twenty-Year Study of Eptesicus Fuscus in Minnesota*. Journal of Mammalogy, Vol. 53, No.1: pp. 201-207.

22. Goodwin, R.A., Politano, M., Garvin, J., Nestler, J., Hay, D., Anderson, J., Weber, L., Dimperio, E., Smith, L. and Timko, M. 2014. *Fish navigate large dams by modulating flow field experience*. Proceedings of the National Academy of Sciences. 111:5277.

23. Gorresen, P. M. et al. 2015. *Behavior of Hawaiian Hoary Bat* (*Lasiurus Cinereus Semotus*) *at Wind Turbines and its Distribution across the North Ko'olau Mountains*, O'ahu, Technical Report, HCSU-064.

24. Gruver, J. and Boros, L. B. 2015. *Summary and Synthesis of Myotis Fatalities at Wind Facilities with a focus on Northeastern North America*, Western Ecosystems Technology.

25. Hall, L. S., and Richards, G. C. 1972. Notes on Tadarida australis (Chiroptera: Molossidae). Australian Mammalogy 1:46.

26. Hatch, S. K., Emily, E. C., Divoll, T. J., Stenhouse, I. J. and Williams, K. A. 2013. *Offshore Observations of Eastern Red Bats* (*Lasiurus Borealis*) *in the Mid-Atlantic United States using Multiple Survey Methods*, Plos ONE 8 (12): e83803.

27. Hayward, B. and Davis, R. 1964. *Flight Speed in Western Bats*. Journal of Mammalogy, 45 (2), 236-241.

28. Hotker, H., Thompson, K. M. and Jeromin, H. 2006. *Impacts on Biodiversity of exploitation of renewable energy sources: the example of birds and bats. Facts, gaps in knowledge, demands for further research, and ornithological guidelines for the development of renewable energy exploitation*, Michael-Otto-Institut im NABU, Bergenhusen, Germany.

29. Howell, J. A., and DiDonato, J. E. 1991. *Assessment of avian use and mortality related to wind turbine operations, Altamont pass, Alameda and Contra counties*, California. U.S. Windpower, Inc., Livermore, California, USA.

30. Hull, C., and Muir, S. 2010. *Search areas for monitoring bird and bat carcasses at wind farms using a Monte-Carlo model*. Australian Journal of Environmental Management 17:77–87.

31. Huso, M. M. P. and Dalthorp, D. 2014. *Accounting for unsearched areas in estimating wind turbine-caused fatality*. The Journal of Wildlife Management, 78 (2): 347-358.

32. Kerns, J. 2005. *Preliminary fatality results – Mountaineer Wind Energy Center, West Virginia*. in Proceedings onshore wildlife interactions with wind developments: research meeting V, November 3-4, 2004, National Wind Coordinating Committee, Lansdowne, Virginia, USA, pp. 18-20.

33. Kingsley, A. and Whittam, B. 2007. *Wind Turbines and Birds: A background review for environmental assessment*. Prepared by Bird Studies Canada Prepared for Environment Canada / Canadian Wildlife Service.

34. Kunz, T. H., Arnett, E. B., Erickson, W. P., Hoar, A. R., Johnson, G. D., Larkin, R. P., Strickland, M. D., Thresher, R. W. and Tuttle, M. D. 2007. *Ecological impacts of wind energy development on bats: questions, research needs, and hypotheses*. Frontiers in Ecology & the Environment. 5: 315–324.

35. Kurta, A. 2001. *Mammals of the Great Lakes Region*. Ann Arbor, Michigan: The University of Michigan Press.

36. Kuvlesky, W. P., Brennan, L. A., Morrison, M. L., Boydston, K. K., Ballard, B. M., and Bryant, F. C. 2007. *Wind energy development and wildlife conservation: Challenges and opportunities*. Journal of Wildlife Management. 71: 2487-2498.

37. Lu, H., Porté-Agel F. 2011. *Large-eddy simulation of a very large wind farm in a stable atmospheric boundary layer*. Physics of Fluids. 23(6): 065101.

38. NAS (National Academy of Sciences). 2007. *Environmental Impacts of Wind-Energy Projects*. The National Academies Press, Washington, D.C., USA.

39. Noberg, U.M. 1976. *Aerodynamics, Kinematics, and Energetics of Horizontal Flapping Flight in the Long-Eared Bat Plecotus Auritus*, J. exp. Biol., 65, 179-212.

40. *Northern Long-Eared Bat Interim Conference and Guidance*, USFWS, January 2014.

41. Oggiano, L. 2014. *CFD simulations on the NTNU wind turbine rotor and comparison with experiments*. Energy Procedia. 58:111.

42. Osborn, R.G., Higgins, K. F., Usgaard, R. E., Dieter, C. D. and Neiger, R. D. 2000. *Bird mortality associated with wind turbines at the Buffalo Ridge wind resource area, Minnesota*. The American Midland Naturalist, vol. 143, pp. 41-53.

43. Politano, M., Dvorak, J. and Laughery, R. 2012. *CFD modeling to reduce fish exposure to TDG and predator habitat at McNary Dam*. Hydrovision International, Louisville, KY.

44. Pruitt, L. and Okajima, J. 2014. *Indiana Bat Fatalities at Wind Energy Facilities*. U.S. Fish and Wildlife Service Bloomington, Indiana Field Office.

45. *Report on Bat Activity in Enfield, NY* 2009. Integrated Environmental Data, LLC, 1330 Bradt Hollow Rd., Berne, NY 12023.

46. Romero-Gomez, P. and Richland, W. A. 2014. *Discrete element modeling of blade-strike frequency and survival of fish passing through hydrokinetic turbines*. Proceedings of the 2nd Marine Energy Technology Symposium METS2014 April 15-18, 2014, Seattle, WA.

47. Salcedo, H. D. C., Fenton, M. B., Hickey, M. B. C. and Blake, R. W. 1995. *Energetic Consequences of Flight Speeds of Foraging Red and Hoary Bats* (*Lasiurus Borealis and Lasiurus Cinereus*; *Chiroptera Vespertilionidae*), J. exp. Biol., 198, 2245-2251.

48. Shrump, A. and Shrump, K. 1982. *Mammalian Species.* The American Society of Mammologists. No. 185.

49. Smallwood, K. S. and Thelander, C. G. 2005. *Bird mortality at the Altamont Pass Wind Resource Area*, final report to the California Energy Commission, Public Interest Energy Research-Environmental Area, 500-01-019, by BioResource Consultants, Ojai, California.

50. *Spatially-Explicit Bat Impact Screening Tool for Wind Turbine Siting*, Versar Inc, 2013.

51. Sørensen, N. and Shen, W. Z. 2002 *Numerical modeling of wind turbine wakes*. J. Fluids Eng. 124: 393.

52. Sterner, D. 2002. *A roadmap for PIER research on avian collision with wind turbines in California*, Public Interest Energy Research P500-02-070F, California Energy Commission, Sacramento, California.

53. Taylor, J. R. A. and Patek, S. N. 2010. *Ritualized fighting and biological armor: the impact mechanics of the mantis shrimp's telson*. The Journal of Experimental Biology, 213, 3496-3504.

54. Thelander, C. G. and Rugge, L. 2000. *Avian risk behavior and fatalities at fatalities at the Altamont Wind Resource Area*, March 1998 to February 1999, NREL/SR-500-27545, National Renewable Energy Laboratory, Lansdowne, Virginia, USA.

55. Thielen, M., Speck, T., and Seidel, R. 2015. *Impact behavior of freeze-dried and fresh pomelo (Citrus Maxima) peel*: influence of hydration state, R. Soc. open sci. 2:140332.

56. Whitaker, J. and Hamilton, W. 1998. *Mammals of Eastern United States. Cornell University Press*: Comstock Publishing Associates.

57. White, F. M. 2009, *Fluid Mechanics*, 7th Edition, *The McGraw Hill Companies*.

58. Winkelman, J. E. 1989. *Birds at a windpark near Urk; bird collision victims and disturbance of wintering ducks, geese, and swans*, RIN-Rappoet 89/15, Rijksinstituut voor Natuurbeheer, Arhem, The Netherlands.

59. Winkelman, J. E. 1992. *The impact of the Sea wind park near Oosterbierum* (*Fr.*), *The Netherlands, on birds, 1: collision victims*, RIN Report 92/2, DLO-Institut voor Bosen Natuuronderzoek, Arnhem, The Netherlands.

60. Yu, Y. and Guan, Z. 2015. *Learning from bat: Aerodynamics of actively morphing wing*. Theoretical and Applied Mechanics Letters (5), 13-15.

61. Zhang, W., Markfort, C. D., and Porte-Agel, F. 2012. *Near-wake flow structure downwind of a wind turbine in a turbulent boundary layer*. Experiments in Fluids, 52 (5), 1219-1235.

62. *Big Brown Bat, Evening Bat, & Little Brown Bat Removal & Control Services*. Blue Ridge Wildlife Management, Accessed June 30, 2016 at http://yourwildlifepro.com/bats.html.

63. Naumann, R. 1999. "*Lasionycteris noctivagans*" (On-line), Animal Diversity Web. Accessed June 30, 2016 at http://animaldiversity.org/accounts/Lasionycteris_noctivagans/.